

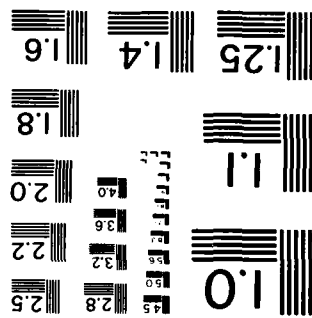
ELECTROMAGNETIC RADIATION FROM CORONA DISCHARGES(U)
DENVER RESEARCH INST COLO ELECTRONICS DIV
H RENO ET AL. 25 JAN 77 DRI-2678 N00019-74-C-0334

NL

F/G 20/3

FLAME TEST

MICROCOPY RESOLUTION TEST CHART
NATIONAL BUREAU OF STANDARDS-1963-A



AD-A148 263

FINAL REPORT
DRI #2678
25 January 1977

REPORT

ELECTROMAGNETIC RADIATION FROM CORONA DISCHARGES

DEC 3 1984

FILE COPY

APPROVED FOR PUBLIC RELEASE
DISTRIBUTION UNLIMITED

UNIVERSITY OF DENVER • DENVER RESEARCH INSTITUTE

84 11 28 034

FINAL REPORT

Electromagnetic Radiation from Corona Discharges

Contract: N00019-74-C-0334

- Sponsored by -

Naval Air Systems Command
Washington, D. C. 20360

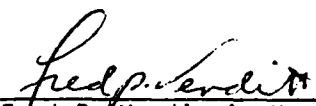
- Performed by -

Electronics Division
Denver Research Institute
University of Denver
Denver, Colorado 80210

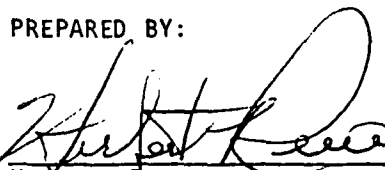
25 January 1977

APPROVED FOR PUBLIC RELEASE
DISTRIBUTION: UNLIMITED

APPROVED BY:


Fred P. Venditti, Head
Electronics Division

PREPARED BY:


Herbert Reno
Senior Research Fellow

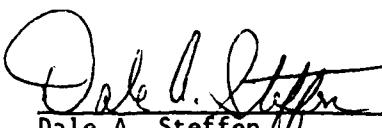

Dale A. Steffen
Research Physicist

TABLE OF CONTENTS

	<u>Page</u>
List of Figures.	iii
I. INTRODUCTION	1
II. EXPERIMENTAL INVESTIGATIONS.	9
A. Measurements on low-flying aircraft	9
B. Investigation of Missiles	14
C. RF energy from a corona point	16
D. Corona from the end of a cylindrical conductor.	18
E. Radio Noise Survey.	27
F. Field measurements above 150 MHz on low flying aircraft.	29
G. Corona measurements at VHF.	31
H. Model aircraft measurements	43
III. ANALYSIS OF RADIATED CORONA PULSE.	51
IV. THEORETICAL DISTANCES FOR CORONA DETECTION	63
V. CONCLUSIONS AND RECOMMENDATIONS.	68
APPENDIX A	76
REFERENCES	79



LIST OF FIGURES

<u>Figure No.</u>		<u>Page</u>
1	Equipment used for ELF measurements	11
2	Equipment used for VLF-LF measurements	11
3	Equipment used for HF measurements	13
4	Vehicle potential vs. altitude	15
5	RF emission from a corona point in air	17
6	Negative point corona current pulse.	19
7	Current distribution on 20 foot pipe	21
8	Corona pulse rate vs. pipe potential	23
9	Charging current vs. pipe potential.	24
10	RF power received from a 10 foot pipe in corona. . . .	25
11	Detected I.F. signals from a 20 foot pipe in corona. .	28
12	Background noise spectrum measured at sea.	30
13	Block diagram of radiometer.	33
14	Revised block diagram of radiometer.	35
15	Equipment set-up for radiometer measurements	36
16	Corona signal amplitude from 0.2m rod, 1 cm diameter .	37
17	Corona signal amplitude from 0.5m rod, 1 cm diameter .	38
18	Corona signal amplitude from 0.5m rod, 5 cm diameter .	39
19	Corona signal amplitude from 1.0m rod, 1 cm diameter .	40
20	Corona signal amplitude from 1.0m rod, 5 cm diameter .	41
21	Corona signal amplitude from 2.0m rod, 1 cm diameter .	42
22	Receiver sensitivity	44
23	Background noise	45
24	Radiometer-helical antenna set-up.	47
25	Model aircraft test set-up	48

LIST OF FIGURES (cont.)

<u>Figure No.</u>		<u>Page</u>
26	Signal amplitude of corona pulses from model aircraft.	49
27	Signal amplitude vs. corona current on model aircraft.	50
28	Calculated current pulse on a cylinder	53
29	Source geometry.	54
30	Radiated pulse from corona electron current in air . .	56
31	Synthesis of radiated pulse train by convolution . . .	60

I. INTRODUCTION

The broad objectives of this program were to conduct an extensive investigation into the sources of static electrification on aircraft and other airborne devices, to identify and study those sources which might be expected to result in significant electromagnetic radiation, to analyze and measure that radiation, and to specify and design instrumentation for the reception and analysis of electromagnetic signals radiated from charged flying objects.

In support of this program a number of tasks were identified and pursued, some casually and some in considerable depth. Certain tasks were proposed as obvious lines of endeavor in the beginning, and others were later added as the study progressed. Some were given only slight attention, either because of the results of others which indicated the desirability of a change in emphasis, or due to lack of time and available funding.

The tasks into which this program was divided are enumerated and briefly described in the following:

1. Literature search on aircraft noise.

This search concentrated on static electricity on aircraft. The data bases from which literature was drawn were the Technology Application Center, the Defense Documentation Center, and the National Technical Information Service. This search was intended to determine static electricity charging mechanisms, as well as the mechanisms which dissipate the accumulated charge.

2. Literature search on static electricity on missiles.

This search was intended to review the literature on static electricity charging and discharging mechanisms on missiles

in order to specify specific areas for later investigation. Possibilities were discovered in the effects of missile firings from aircraft and the effects of a missile breaking water.

3. Measurement equipment configuration.

This task consisted of the assembly and reconfiguration or modification of existing equipment for preliminary measurements on low-flying commercial aircraft in the ELF, VLF, LF, and HF frequency bands.

4. Measurements on low-flying aircraft.

The equipment assembled in Task 3 was employed to make measurements on low-flying aircraft in the ELF, VLF, LF and HF bands. The results of these measurements indicated that any electromagnetic signals generated in these frequency bands are well below the background noise level. Theory indicates that any signals in these bands exhibit very random characteristics in addition to being of relatively low amplitudes, and therefore would be very difficult to detect in the presence of background noise.

5. Theoretical investigation of radiation from corona discharge.

A theoretical study was conducted to develop a theory of the corona discharge mechanisms which would define the time and frequency characteristics of corona discharge to aid in the prediction of radiated signals. The difficulty encountered in calculating the effects of the airframe on the radiation mechanisms led to the conclusion that field measurements were required in order to obtain any reliable data on the nature of the radiated signal.

6. Reconfiguration and calibration of VHF equipment.

Existing measuring equipment and systems were reassembled and calibrated to make field measurements in the VHF frequency band. The objective was to make measurements of the radiated corona pulse in close proximity to an aircraft, and to measure typical background noise levels at sea.

7. Measurement of corona pulse characteristics.

Laboratory measurements were made of the radiated pulse shapes from small bodies in corona to support the theoretical studies undertaken in Task 5.

8. Measurements of background noise levels at sea.

It was originally intended to make measurements of the possible radiation from missiles fired at sea, but scheduling problems never permitted these measurements to be carried out. However, an attempt was made to obtain background noise data from a quiet ship at sea. These measurements were made aboard the Acania, but they were inconclusive because of the limited distances from shore which could be reached.

9. Corona measurements on aircraft and missiles.

The intent of this task was to perform, repeat, and refine close proximity corona measurements to supply the required data for the theoretical investigation of corona discharge. It was then intended to extend the task to include far-field measurement of corona discharge effects. These measurements were intended to include the dependence of the radiated signal on a variety of parameters, including, for example, aircraft speed and altitude.

10. Investigation of precipitation static on missiles.

This task was intended to conclude the literature search on missile static in order to furnish sufficient background on the radiation mechanisms to permit an assessment of the possibilities of their employment as a means of detection. It was intended to obtain radiation measurements from missiles being fired from aircraft, ships, and land-based launchers.

11. Investigation of streamer discharge and arcing on aircraft.

This task recognized that these phenomena are less likely to occur than corona. However, it was intended to attempt to locate the sources of streamer and arcing, and then to make measurements. The measured data would then be compared with any available analysis in order to determine the extent of electromagnetic radiation from these mechanisms.

12. Investigation of microwave noise generated by triboelectric charging.

This task was added because the general literature searches revealed references to work performed on this mechanism. The intent was to review these references with particular attention to the existence of radiated signals, and subsequently to make a detailed study of microwave noise and available instrumentation.

13. Investigation of other sources of electromagnetic radiation from airframes.

This investigation was to be guided by the information obtained from literature searches, the availability of measuring instrumentation, and previous results obtained from analysis and measurement experiments. Examples of possible

activities under this task were:

- a. Investigation of signals generated by arc suppressors located on aircraft which are passing through storm cells or other lightning-generating environments.
- b. Under the assumption that field observations of corona effects indicated that radiation was measureable and distinguishable from background noise at significant distances, a task was to be added to investigate the effects of various types of static dischargers. It was intended to determine those kinds of discharges which exhibit low-level radiation and those types which produce high-level radiation.
- c. Investigation of the properties of missile exhaust discharge radiation. This task was added since references were found which indicate that the missile body acts as an antenna array and therefore imparts a directional characteristic to the radiation. An attempt was to be made to determine the nature of this radiation pattern and to correlate it with missile configuration. This effort was to include an investigation of arcing from the missile mainframe to the missile exhaust.
- d. Investigation of the properties of charged water droplets formed when a missile breaks water.

14. Instrumentation specification.

It was expected that the results of the above tasks, both theoretical and experimental, would permit the selection of the most promising radiation mechanism or mechanisms, and that

this would provide the basis for the specification of specialized instrumentation. Such specifications would be based on the characteristics of the radiated signal and would therefore define required frequency ranges, bandwidths, dynamic ranges, and signal-to-noise ratios. Depending primarily on signal-to-noise ratios it was expected that equipment philosophy could vary from brute-force methods at high S-N ratios through filtering with wide-band circuits, filtering with narrow-band circuits, sampling, correlation techniques, and integration techniques at very low S-N ratios.

15. Design of an integrating noise receiver.

This task was undertaken during the latter stages of the project. In the course of pursuing earlier tasks, measurements of the radiation from bodies in corona discharge were limited to relatively close distances of the order of fifty feet by not only noise background but by the sensitivity of available equipment. Data obtained in earlier measurements indicated that fields radiated by corona could be detected at much greater ranges with an integrating noise receiver known as a radiometer. The results previously obtained appeared sufficient to allow the specification of such a receiver, and accordingly its design was undertaken.

16. Construction of aircraft models.

Measurements of corona discharge on previous tasks were largely made on cylinders with length-to-diameter ratios of 50:1 and 100:1, ratios which are not representative of typical aircraft and missile airframes. It was therefore decided to construct a crossed-cylinder airframe model of a KC-135

aircraft with lengths of wings, fuselage, and tail section scaled 20:1. It was intended to employ the radiometer receiver to study the radiated fields generated by corona occurring at various locations along the trailing edges of the wings and tail sections. Measurements were planned at frequencies near the airframe resonances and in a frequency range well above the highest significant resonance. It was hoped that the frequency spectrum of the aircraft corona radiation could be obtained to several hundred megahertz, and that the spectrum frequency dependence above all resonances could be determined. It was then the intention to scale these data to an actual aircraft, to obtain data on typical integrated background noise levels at a variety of locations with the radiometer, and thereby to predict the possibilities of detection of corona signals from actual aircraft using radiometric techniques.

17. Radiometer measurements.

After completion of the radiometer design and construction, a number of attempts were made to use it to make measurements of corona both from cylindrical rods and from the aircraft model. However, no locations were found in the Denver area, including inside the metal structure at the Cherry Creek Field Site, where the background noise was not sufficiently intense and variable to preclude obtaining any significant results. Therefore, those measurements which were made were done using the radiometer as a conventional low-noise receiver. It was planned to attempt further radiometer measurements on the aircraft model in a fully shielded room, but

contract time and fund limitations prevented that project from being undertaken.

In summary, although the initial objectives of this project were very broad, the early phases strongly indicated that the only likely source of aircraft or other airframe radiation which is sufficiently intense and at the same time satisfactorily dependable and repeatable to allow the possibility of detection at reasonable distances was that due to corona discharge. Since it was decided that the emphasis of the program should be on a study of the far-field radiation arising from electrification of the aircraft rather than on the on-board effects of static discharge, major attention was devoted to corona and possible means of detecting an aircraft undergoing corona discharge. The activities of the project were therefore centered on a theoretical analysis of corona discharge, on measurements of corona radiation in the close proximity of simple geometries in corona, on measurements of aircraft models, and on an attempt to employ radiometer noise receivers for the detection of corona radiation.

II. EXPERIMENTAL INVESTIGATIONS

This section of this report describes those measurements which were made and the results which were obtained in the pursuance of Tasks 4, 7, 8, 9, and 17 as outlined in Section I.

A. Measurements on low-flying aircraft

The results of the literature searches which were conducted indicated that the primary sources of static electrification on aircraft were:

- a. Corona discharge
- b. Streamer discharge
- c. Charge acquisition in an antenna region due to impact of individual particles.

The first two sources were found to be the only ones which might result in significant electromagnetic radiation. Streamer discharge was found to be only of secondary interest because it rarely occurs in clear air, is hard to distinguish from atmospheric radiation from storm cells, and since preventive techniques exist which eliminate it as a significant source during most atmospheric conditions encountered in flight. However, corona discharge was found to exist for nearly all flying conditions; therefore, the almost continuous presence of this source of static electrification, together with an essentially repeatable waveform shape and a repetition rate on the order of 10^5 pulses per second, rendered it of considerable interest. As a result, more detailed investigations were made to determine the nature of the electromagnetic radiation expected from corona. The frequency range of interest from corona discharge is in the band of 10 MHz to 200 MHz. Therefore this frequency band was the subject of more intensive investigation in later tasks.

Once corona discharge was singled out for special investigation, experiments were conducted to identify other possible sources not mentioned

in the literature. This investigation consisted of an attempt to obtain empirically any radiated signals from aircraft in the frequency range below the one of interest mentioned above. Since it was not known what signal characteristics to expect in the time domain, steady-state frequency measurements were made. The three separate frequency ranges which were considered were:

- a. 10 Hz to 300 Hz (ELF)
 - b. 5 kHz to 1 MHz (VLF-LF)
 - c. 3 MHz to 30 MHz (HF)
1. ELF Measurements

Figure 1 is a block diagram of the equipment used to make ELF measurements. Observation of the oscilloscope display during the presence and absence of low-flying aircraft constituted the data measurement in the ELF band. The measurements were made very close to, and often directly beneath, aircraft flying at an altitude of approximately 100 feet. The observed signal in the presence of an aircraft appeared to be a sinusoidal wave of roughly 10 Hz with an approximate amplitude of 50 mv/meter. The fundamental and harmonic components of 60 Hz radiated from nearby power lines produced a measured background signal of approximately 100 mv/meter, and if higher ELF frequency components were radiated by the aircraft they were not detectable in the presence of this background noise. Since the 10 Hz signal was observed from aircraft only when they were very near the receiving antenna, it is concluded that the signal was due to the static field of the aircraft and would not produce useful signals at any appreciable distances.

2. VLF-LF Measurements

Figure 2 is a block diagram of the equipment used to make VLF-LF measurements. The oscilloscope was used to observe signals in the

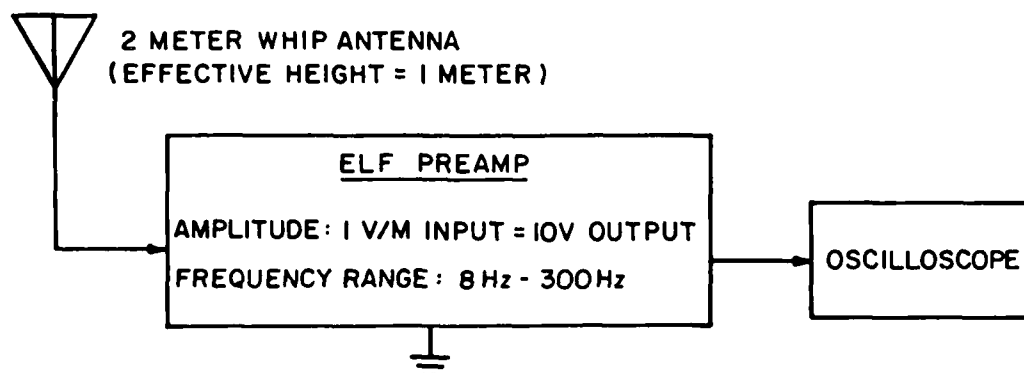


FIGURE 1. EQUIPMENT USED FOR ELF MEASUREMENTS

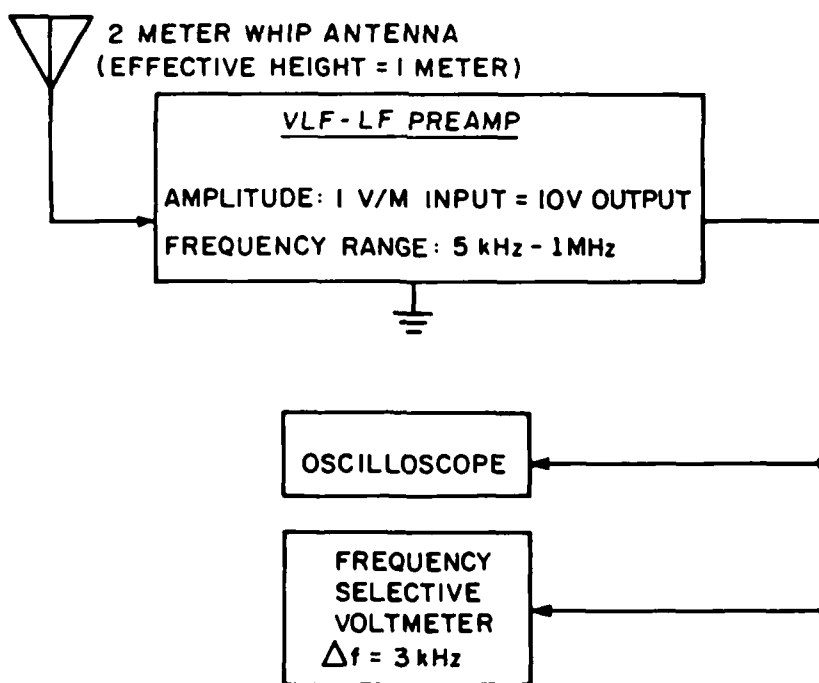


FIGURE 2. EQUIPMENT USED FOR VLF - LF MEASUREMENTS

time domain, while the frequency selectable voltmeter was used to monitor 3 kHz bandwidth measurements. The center frequency could be varied from 5 kHz to 1 MHz. Measurements were attempted of aircraft flying at an average altitude of 500 feet. The average line-of-sight distance from the aircraft to the antenna was 1200 feet. Although some impulsive activity could occasionally be seen above the noise background during an aircraft fly-by, the same type of activity could be seen in the absence of aircraft as well. No steady-state increase could be seen. Also, the AM broadcast stations in the area presented such a strong background signal that virtually no conclusions could be drawn concerning electromagnetic radiation from aircraft in this frequency band.

3. HF Measurements

Figure 3 is a block diagram of equipment used to make HF measurements. The loop antenna was placed in the same location as the VLF-LF whip antenna. Again no increase was observed in the steady-state signal level of the envelope detector during aircraft fly-by. Impulsive noise always appeared to be present during an aircraft fly-by for frequencies above 20 MHz, whereas in the absence of aircraft this impulsive noise was not always present. This observation may be purely coincidental, however, since it was impossible to monitor any one frequency setting for more than a few aircraft fly-bys in order to make measurements over the entire frequency range.

4. Conclusions

This investigation indicated that if any electromagnetic radiation does exist in the frequency bands considered, it is of lesser amplitude than the average background noise level. Since there is nothing in the literature which presents specific time-dependent waveform shapes with these frequency components except streamer discharge, it is difficult to design more specific measurements in these frequency bands. It was therefore concluded that primary effort should be devoted to corona discharge.

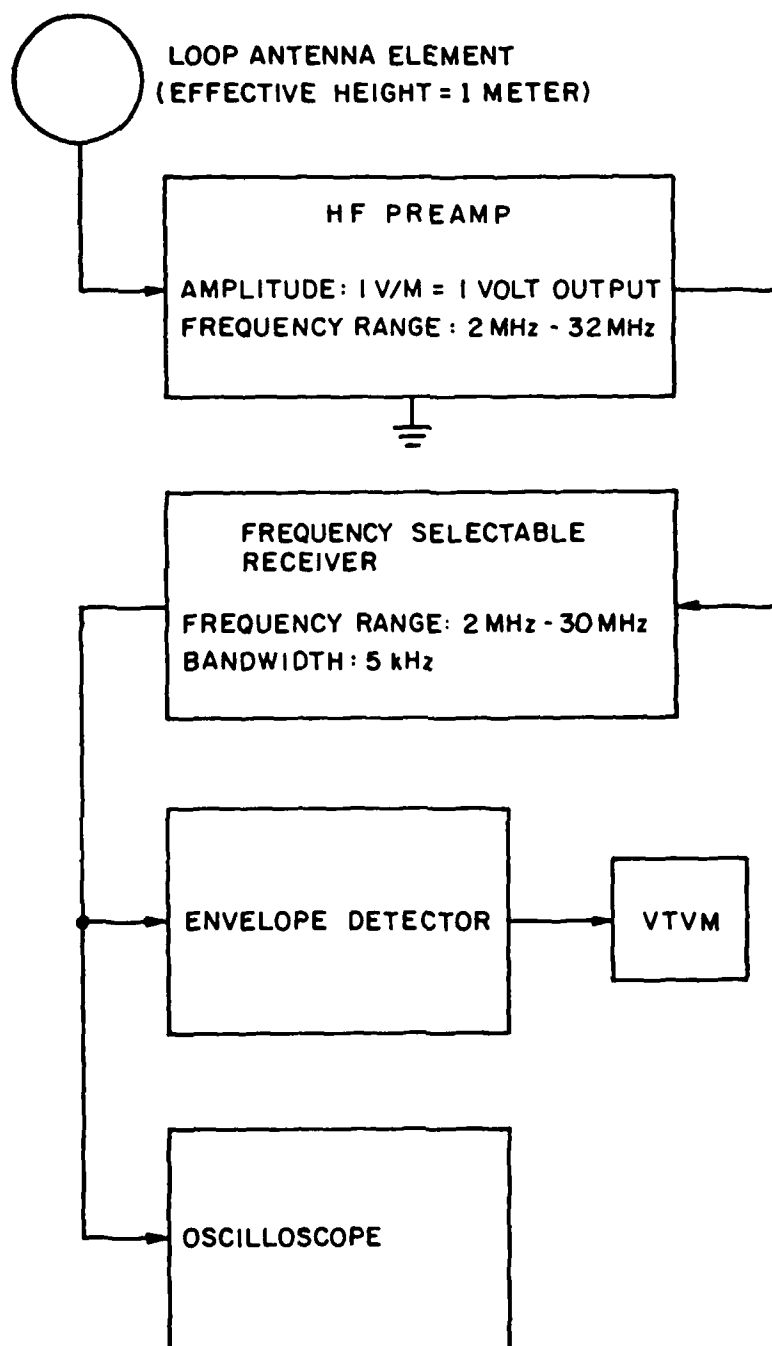


FIGURE 3. EQUIPMENT USED FOR HF MEASUREMENTS

B. Investigation of Missiles

Although the charging mechanisms present in missiles vary from those in aircraft, the discharge mechanisms are nearly the same. One exception is that the exhaust plume of the missile may serve as a discharger (rather than a charger) at certain altitudes. This is because missile exhaust leaves a net positive charge on the missile, while triboelectric charging leaves a net negative charge on the missile. Therefore, at altitudes where triboelectric charging can occur, the exhaust plume tends to neutralize or discharge the missile.

The primary discharge of static electricity appears to be corona discharge. As with aircraft, proper techniques essentially eliminate streamer discharging. Therefore, the conclusion again is that it is of interest to study corona discharge since it also exists on missiles a great deal of the time while a missile is in flight.

As mentioned above, the rocket motor exhaust, or plume, serves as both a charger and a discharger, the particular function being altitude dependent. The result is an altitude dependence of potential (and therefore of electrostatic charge) on the missile. Figure 4, which illustrates this, was encountered while reviewing the available literature.¹ This figure triggered an interest in missiles fired from aircraft, since prior to a firing such a missile must be maintained at the same potential as the aircraft. Nanevicz² et al have shown that even aircraft with dischargers possess corona threshold potentials on the order of 20 kilovolts. This implies that the potential in Figure 4 just prior to Cajun ignition is approximately the poten-

¹ J.C. Axtell and T.C. Oakberg, "An Electrostatic Charge Phenomenon Associated with Minuteman Missile Flights," Lightning and Static Electricity Conf., December, 1968.

² J.E. Nanevicz, E.K. Vance, R.L. Tanner, G.R. Hilbers, "Development and Testing of Techniques for Precipitation Static Interference Reduction," SRI Final Report, Project 2848, Contract AF-33(616)-6561, January 1962.

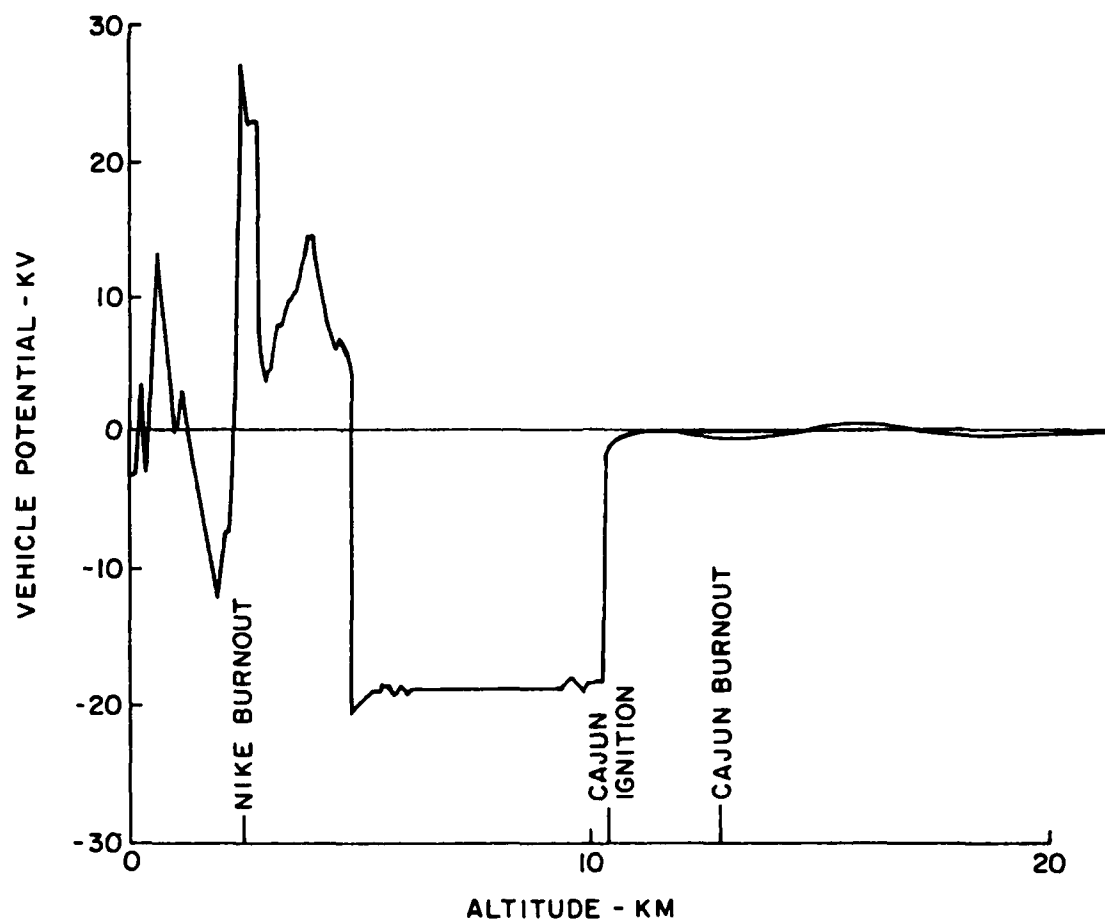


Figure 4. Vehicle Potential Vs. Altitude.
Nike-Cajun Electrostatic Charging Experiment.

possess corona threshold potentials on the order of 20 kilovolts. This implies that the potential in Figure 4 just prior to Cajun ignition is approximately the potential on a missile attached to an aircraft prior to firing. If upon firing the missile, the discharge phenomena displayed in Figure 4 occurs, significant electromagnetic radiation may result. At this time, insufficient literature exists to explore this mechanism as a possible source. Therefore, as a part of Phase II, further investigation of

tial on a missile attached to an aircraft prior to firing. If, upon firing the missile, the discharge phenomena displayed in Figure 4 occurs, significant electromagnetic radiation may result. At this time insufficient literature exists to explore this mechanisms as a possible source.

C. RF Energy from a Corona Point

An investigation of the power radiated in the 30 MHz to 9 GHz frequency range by corona point discharges in air was carried out at the Cherry Creek Field Site southeast of Denver after a receiving system was assembled from available components. The system utilized an HP8555 Spectrum Analyzer as the receiver and various electric field probes and microwave horn antennas as sensors. The system sensitivity was approximately -90 dbm for a 300 kHz bandwidth, the widest bandwidth available on the HP8555 analyzer. The experiments were performed inside a shielded metal building to reduce the interference from commercial radio transmissions.

R-f energy at frequencies below 150 MHz was found to be detectable at a distance of 1 meter from the corona point with this recording system. However, no signal power could be detected at higher frequencies due to the relatively high level of internal system noise above 150 MHz.

The microwave measurements were repeated at Fort Huachuca, Arizona, using equipment with a better signal to noise ratio and a wider bandwidth. This receiving system utilized a Microtel receiver with a 20 MHz bandwidth for the 1 to 10 GHz frequency range and a Watkins-Johnson receiver with a 3 MHz bandwidth to cover frequencies below 1 GHz. Various TWT preamplifiers were used to increase the system gain.

R-f energy from the corona point was found to be detectable with this receiving system over the entire frequency range studied. The results are shown in Figure 5 as a function of frequency, with the measurements below

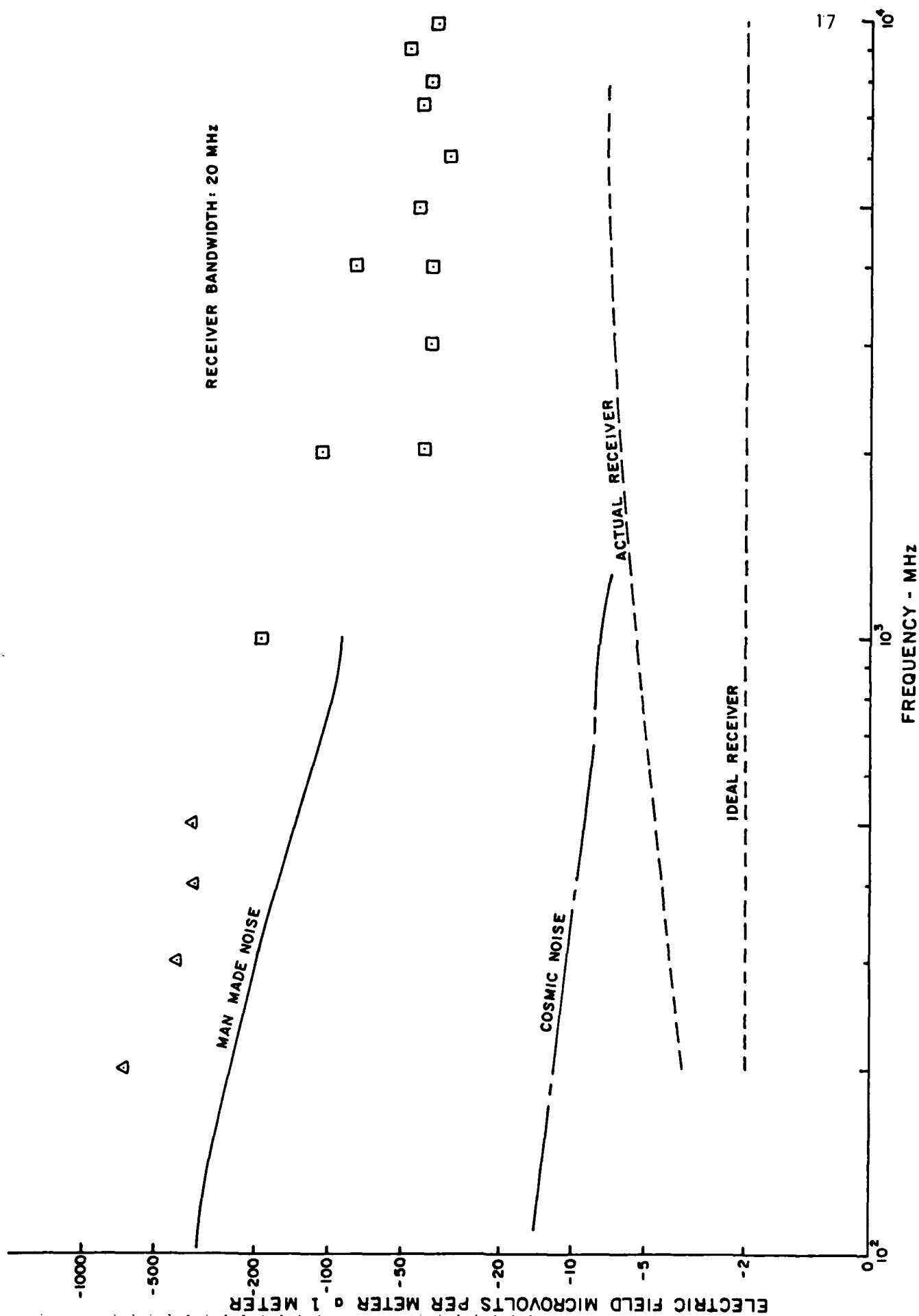


FIGURE 5. R-f EMISSION FROM A CORONA POINT IN AIR

1 GHz scaled as $\sqrt{20/3}$ to account for the different bandwidths used. Actual measurements at different bandwidths indicated that the signal amplitude increased with bandwidth somewhat more than proportional to the square root of bandwidth.

The corona current was monitored during the experiments by measuring the voltage pulse across a 50 ohm high frequency disk resistor. A typical current pulse recorded with a Tektronix R7912 Transient Digitizer with a rise time of approximately 1 nanosecond is shown in Figure 6 for negative point corona.

D. Corona from the end of a cylindrical conductor

1. Description of experiments

Experiments were performed on 10 and 20 foot lengths of 2-1/4 inch diameter aluminum pipe with the following objectives:

- a. Verify the pulsed transmission line model of the current distribution.
- b. Measure the corona repetition rate and d.c. charging current as a function of the charging voltage.
- c. Measure the radiated power in the far zone ($d > 1.2 \times$ wavelength) of the cylinder.

The work was done at the Cherry Creek Field Site with the pipe supported horizontally or vertically by an insulated stand. One end of the pipe was capped with a spherical conductor and the other was tapered to a point. Voltages of up to -50 KV were applied through a charging coil so that any transient current pulses initiated by a corona discharge at one end would travel on the pipe rather than through the power supply.

2. Current distribution

The current distribution on the pipe was measured by mounting the 20 foot pipe horizontally 1 meter above a wire mesh ground screen

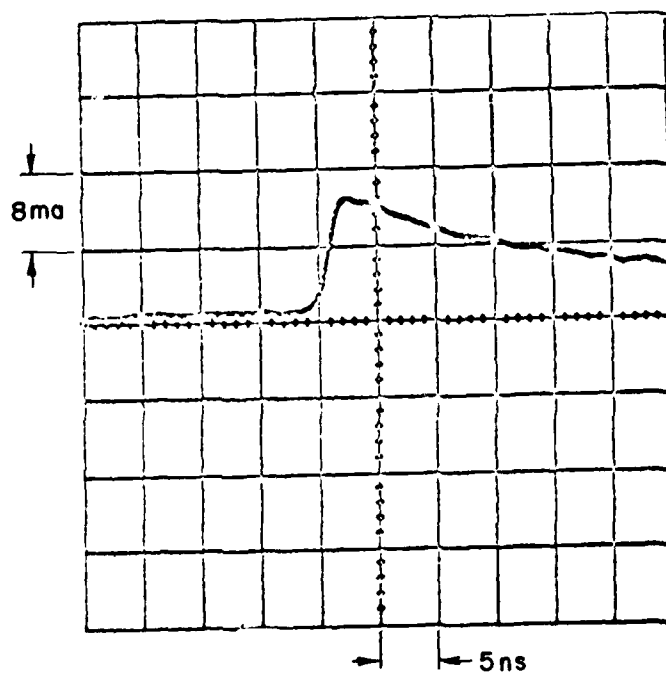
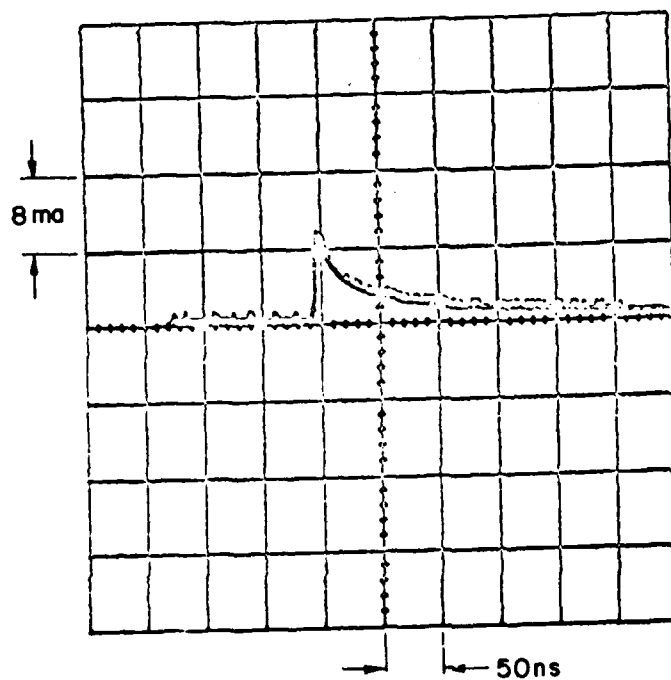


FIGURE 6. NEGATIVE POINT CORONA CURRENT PULSE

and recording the radial electric field at the ground directly below the pipe. For this geometry the radial electric field and current are related by the equation

$$e(t) = \frac{120i(t)}{h}$$

where h is the distance to the ground plane.

The E-field measurements were made with a short probe antenna which fed a high impedance preamplifier, followed by a 40 MHz high-pass filter to reduce the background noise from commercial radio transmissions. The output was recorded on film with a Tektronix 454 oscilloscope. The overall system passband was 40 to 150 MHz for this experiment.

Measurements were obtained with the probe at distances of 4, 8, and 12 feet from the corona point. The results are shown in Figure 7, together with the system response to a step function of voltage. The initial pulse and reflections from the open ends of the pipe are seen to occur as expected. The reflection time delays correspond to the pulse travel time from the observation point to the ends of the pipe and back at approximately the speed of light. The system sensitivity was such that a field strength of 3.3 volts/meter corresponded to 1 volt deflection on the oscilloscope. The 170 mv amplitude of the first pulse corresponds to a current pulse of 5 milliamps. The first reflection from the end of the pipe arrived before the initial pulse had died out completely. This distorted the amplitude of the reflected pulse; however the distortion is low at the 4 foot position where the time separation is maximum. The ratio of the reflected to initial pulse amplitude at this point gives a reflection coefficient of approximately 0.8. The reflection coefficient would be unity in the ideal case.

3. Corona pulse rate and charging current

The corona pulse rate and d.c. charging current on the 20 foot

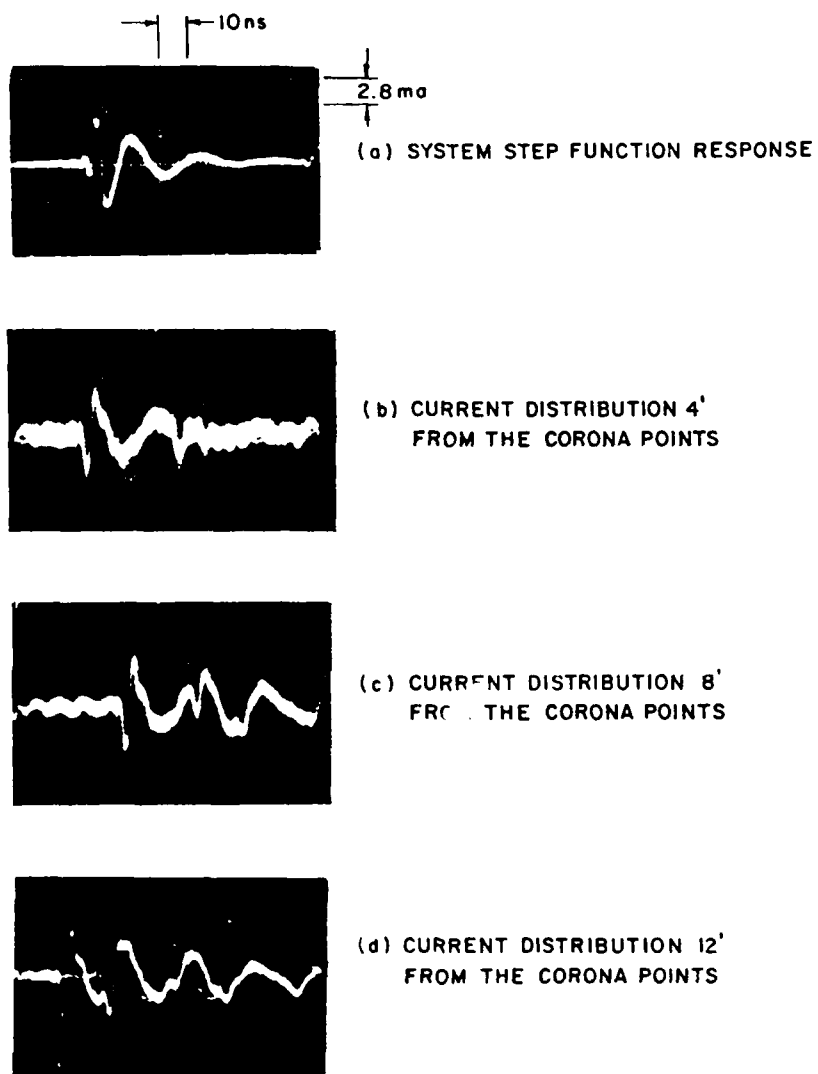


FIGURE 7. CURRENT DISTRIBUTION ON 20' PIPE

pipe were measured at pipe voltages between -6 KV and -30 KV. Trigger pulses were picked up from a small metal plate placed approximately 10 cm from the corona point and grounded through a 50 ohm resistor. The voltage pulse across the resistor caused by induced current in the plate was amplified and used to trigger an electronic counter.

The average pulse rate as a function of the charging voltage is shown in Figure 8. The rate increases sharply once the corona threshold voltage of approximately -5 KV is exceeded.

The charging current and average current per pulse as a function of voltage are shown in Figure 9. The increase in the average current per pulse as the voltage increases is consistent with an expected increase in the number of electron avalanches per pulse as the field energy increases.

4. RF radiation

The power radiated by vertical 10 foot and 20 foot lengths of pipe was measured at distances of 25 and 50 feet. At these distances the far field is a factor of 10 greater than the near field at frequencies above 47 MHz at 25 feet and 24 MHz at 50 feet. The measurements were made with a log-periodic antenna with a gain of 12 db, designed for the 30 to 300 MHz frequency range. The instrumentation consisted of a low noise preamplifier, 150 feet of RG-8 coax cable, and an HP8555A Spectrum Analyzer. The data were recorded by photographing the display scope of the spectrum analyzer when it was operated in a swept-frequency mode, or by photographing the detected I.F. output on an auxilliary oscilloscope when it was operated as a fixed-tuned receiver. The system, excluding the antenna, was calibrated with a VHF signal generator over the 10 to 480 MHz frequency range.

Swept frequency recordings of the power received in a 300 kHz pass-band from the 10 foot pipe are shown in Figure 10. The upper trace (a)

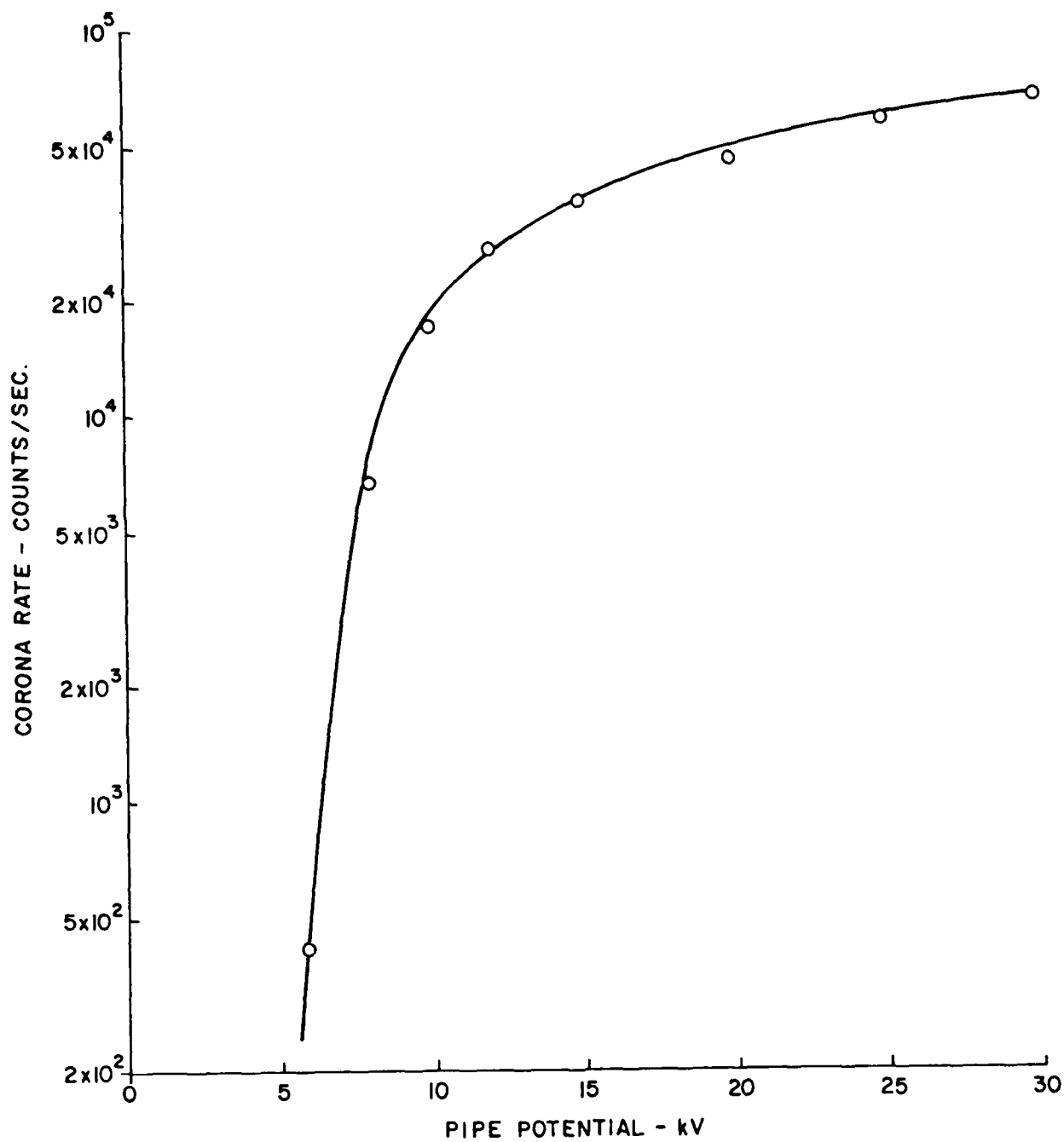


FIGURE 8. CORONA PULSE RATE VERSUS PIPE POTENTIAL

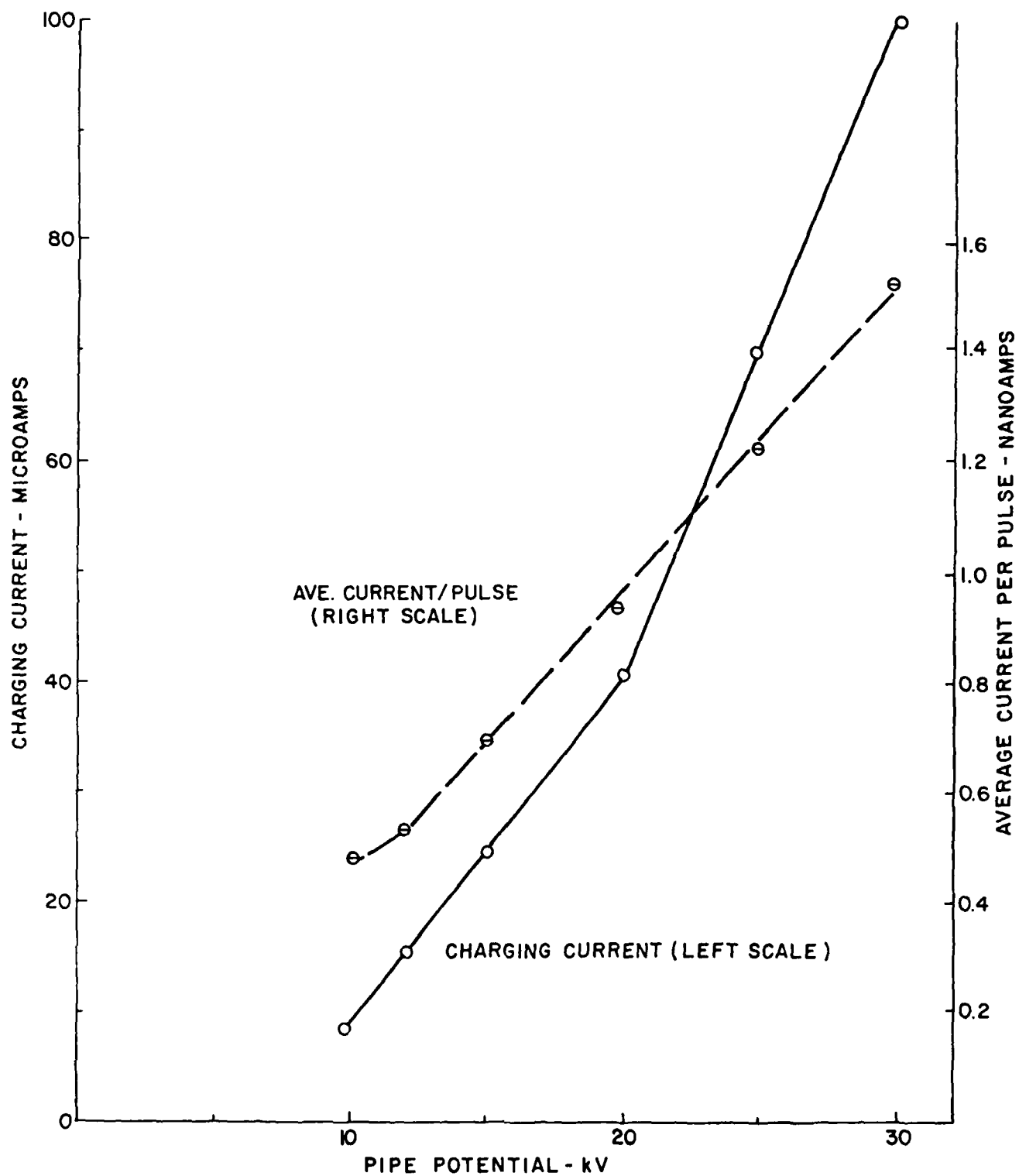
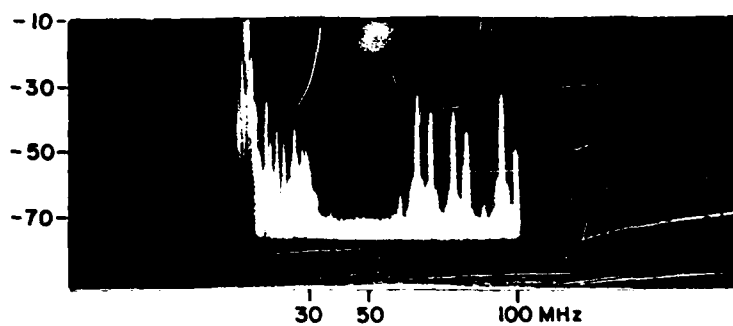
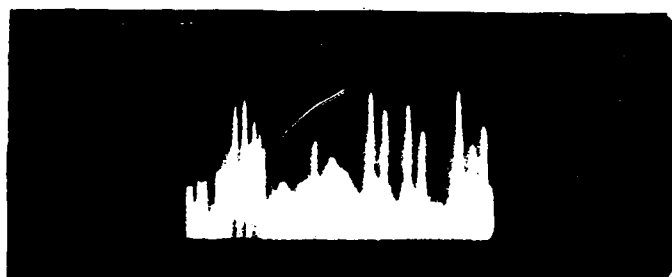


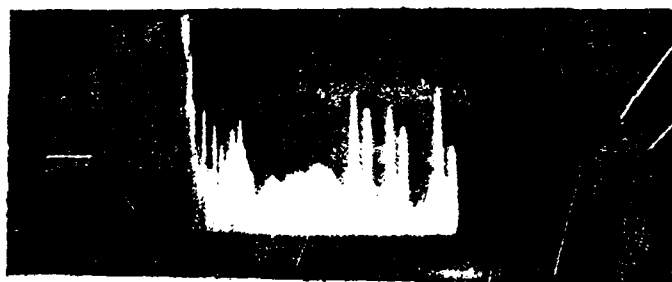
FIGURE 9. CHARGING CURRENT VERSUS PIPE POTENTIAL



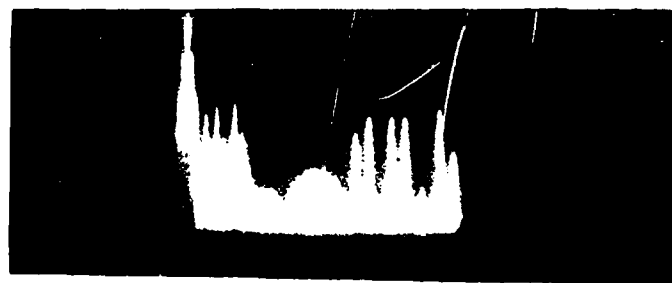
(a) BACKGROUND NOISE (dbm)



(b) CORONA NOISE AT 25'
SINGLE POINT AT TOP



(c) CORONA NOISE AT 25'
SINGLE POINT AT BOTTOM



(d) CORONA NOISE AT 50'
SINGLE POINT AT BOTTOM

FIGURE 10. R-f POWER RECEIVED FROM A 10' PIPE IN CORONA

shows the normal background noise level at the Cherry Creek Field Site with a fairly quiet zone between approximately 25 and 60 MHz. Trace (b) was recorded at 25 feet with a single corona point at the upper end of the pipe. The lower spherically capped end was 24" above ground level. Traces (c) and (d) show the noise power at 25 feet and 50 feet respectively with the corona point at the lower end of the pipe.

The pipe potential was held at -25 KV for these experiments. A broad spectrum of corona noise is seen at levels 15 to 20 db above the background level over the 25 to 60 MHz frequency range where the background is low (-75 dbm). The reduction in peak amplitude of approximately 6 db between the 25 foot and 50 foot recording distances is consistent with the expected 6 db change that should occur in the radiation zone when the distance is doubled. No significant differences are observed between traces (b) and (c), which correspond to corona from the top and the bottom of the pipe.

The power measurements obtained with the spectrum analyzer are related to the incident field by the equation

$$E_i = \frac{5.7 \times 10^{13} f_o \sqrt{P}}{g}$$

where E_i = spectral amplitude of the incident field (v-sec/m),

f_o = receiver center frequency (Hz),

P = recorded power (watts),

g = voltage gain of the receiving system.

The equation above is based on the assumption that the spectral amplitude E_i is constant over the receiver pass band and that the antenna gain is 12 db. As an example, a recorded power level of -60 dbm at a frequency of 50 MHz corresponds to an incident field of 3×10^{-10} v-sec/m with a system voltage gain of 3.

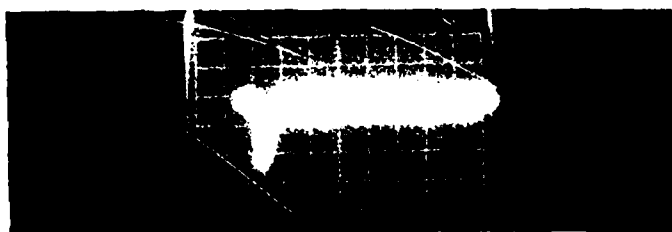
Strong interference at frequencies above 60 MHz prevented measurement of the corona spectrum at higher frequencies using the swept frequency mode. However, with the receiver tuned manually to frequency points where the interference was relatively low, the corona noise could be detected by observing the detected I.F. output of the spectrum analyzer. With this technique, corona noise could be observed at frequencies up to approximately 120 MHz. Examples of the detected output in a 300 kHz pass band are shown in Figure 11 for center frequencies of 30, 50, 75, and 100 MHz. These data were recorded at a distance of 25 feet from the 20 foot pipe, which was held at a potential of -8 KV.

The data presented here were all recorded with the radiating structure and receiving antenna oriented vertically over soil of average conductivity. The fields are therefore approximately doubled over those that would be observed from the same structure in the absence of the ground. Some attempts were made to record the corona noise with the antennas parallel to the ground; however, the ground reflected signal in this case nearly cancels the direct signal after a time delay which is proportional to the ray path difference between the direct and ground reflected field components. The time delays for the source-receiver geometries that could be practically attained were only a few nanoseconds and no data were recorded from the horizontal configuration.

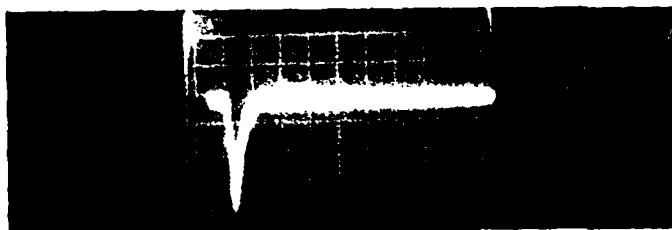
E. Radio Noise Survey

1. Description of experiments

Experiments designed to measure the natural noise background in the 30 to 350 MHz frequency range were carried out aboard the R/V Acania, a research vessel operated by the Department of Oceanography of the Naval Postgraduate School, Monterey, California. The primary goal was to record



(a) 30 MHz CENTER FREQUENCY
0.1 mv/div
5 μ s/div



(b) 50 MHz CENTER FREQUENCY
0.1 mv/div
5 μ s/div



(c) 75 MHz CENTER FREQUENCY
0.05 mv/div
5 μ s/div



(d) 100 MHz CENTER FREQUENCY
0.05 mv/div
5 μ s/div

FIGURE II. DETECTED I.F. SIGNALS RECEIVED FROM A 20' PIPE IN CORONA

the broadband impulsive background noise at sea, with a secondary objective of measuring background noise at narrower bandwidths on a swept frequency basis.

The broadband measurement system consisted of a short vertical monopole antenna which fed a high impedance preamplifier, pulse amplifiers, and a Tektronix 485 oscilloscope. The system pass band was 30 MHz to 450 MHz. The narrow band swept frequency system utilized a log-periodic antenna and a HP8555A spectrum analyzer which covered the 50 to 500 MHz frequency range.

2. Results

The experiments were performed in July 1975 at a maximum distance from shore of 120 miles. Figure 12 shows a typical swept frequency plot of the noise received in a 300 kHz pass band using the narrow band system. Man-made noise at levels of -100 to -120 dbm predominated at this distance from shore over much of the frequency range studied. At closer distances the noise was higher and consisted solely of man made signals.

Measurements of the impulsive background noise were unsuccessful because of the limited distance from shore of the Acania. Television and/or FM broadcast station signals at the maximum distance of 120 miles were still much stronger than the impulsive background noise at this distance.

F. Field Measurements Above 150 MHz on Low Flying Aircraft

1. Description of Experiments

The measurement of noise generated by aircraft in flight was attempted with available instrumentation after modifying the HP8555A spectrum analyzer to give a 10 MHz I.F. bandwidth. The recording system, using the log-periodic antenna, was set up at a distance of 100 meters south of the east end of the East-West runway at Stapleton International Airport in Denver. Observations were made on several occasions during varied weather conditions.

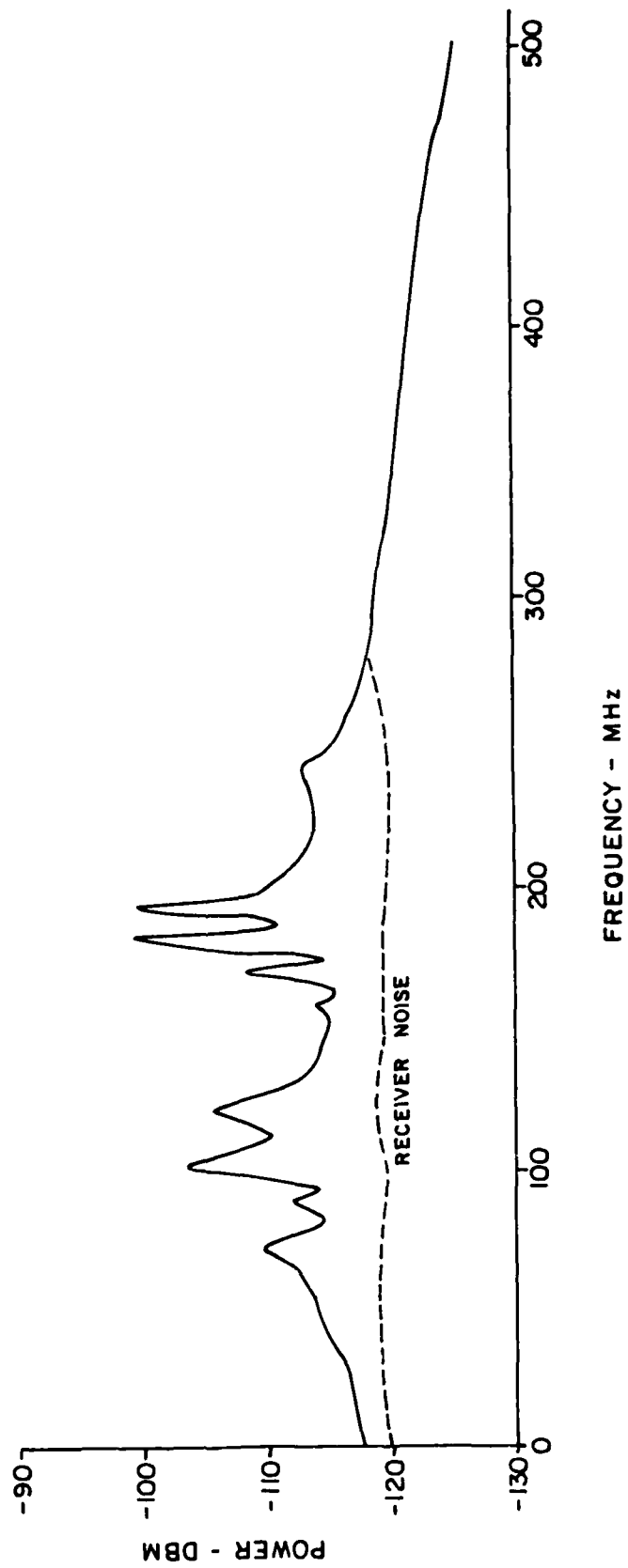


FIGURE 12. BACKGROUND NOISE SPECTRUM MEASURED AT SEA

The analyzer was tuned to relatively quiet frequency spots near 150 MHz or 275 MHz and the I.F. output was monitored on an oscilloscope.

2. Results

Signals consisting of bursts of random appearing pulses, often accompanied by a short quasi-CW burst, were observed on several occasions as aircraft flew through the antenna beam. The most consistent observations were obtained during a two-hour period when light rain was falling. Nearly all of the aircraft gave detectable signals during this period, whereas only the larger aircraft such as DC-10's or 747's were detectable during balmy weather. It was observed that automobile ignition noise was generally detectable at considerably greater distances than were aircraft.

Although these experiments involved a large number of variables which could not be controlled, strong correlation was observed between the passage of an aircraft through the antenna beam and the noise output of the recording system. However, the recorded noise could not be definitely attributed to corona as no independent method was available to determine whether or not the aircraft were actually in corona at the time the observations were made.

G. Corona Measurements at VHF

1. Instrumentation

Additional measurements of radiation from bodies in corona were made over the frequency range of 30-520 MHz. Below are listed the types of antennas employed for the various frequency bands.

Frequency	Antenna	Gain in db over isotropic
30-400 MHz	6" monopole	22*
50-500 MHz	Log periodic	11
300-520 MHz	End-fire helix	10

*Includes preamplifier at base of antenna

Narrowband measurements were made with the Hewlett-Packard Spectrum Analyzer. Wide band measurements above 450 MHz were made with a Microtel Receiver. Wideband measurements from 50 to 450 MHz were made using a low-noise receiver, originally conceived as a radiometer, designed and built at DRI in conjunction with an oscilloscope or a transient digitizer.

Early measurements of RF radiation from conducting cylinders undergoing corona discharge were limited to relatively close distances of the order of 50 feet by the sensitivity of available equipment. The data obtained from those measurements indicated that the radiated fields could be detected at much greater distances with an integrating type noise receiver called a radiometer. Findings in earlier experiments were sufficient to allow specification of the required instrument. The radio noise survey specified the required noise figure of the device. Also, the measurements of RF energy from corona points justified the source function used in the theoretical analysis of the radiated fields from conducting cylinders in corona discharge. Calculated results obtained from the theoretical analysis coupled with experimental measurements specified the operating frequency range, required gain, and approximate integrating time constant. The necessity of designing and developing a radiometer became apparent when it was found that the required specifications were not readily obtainable in off-the-shelf equipment.

Figure 13 is the block diagram of the radiometer as originally specified. The operating frequency range is 30-500 MHz with a 2.5 db noise figure. An input switch is provided to allow switching between the input signal and a known noise source for amplitude calibration. The Avantek pre-amplifiers achieve the necessary noise figure, and the voltage tuned oscillator provides the necessary tuning capability over the desired frequency range. The noise figures of all components after the first I.F. amplifier are not

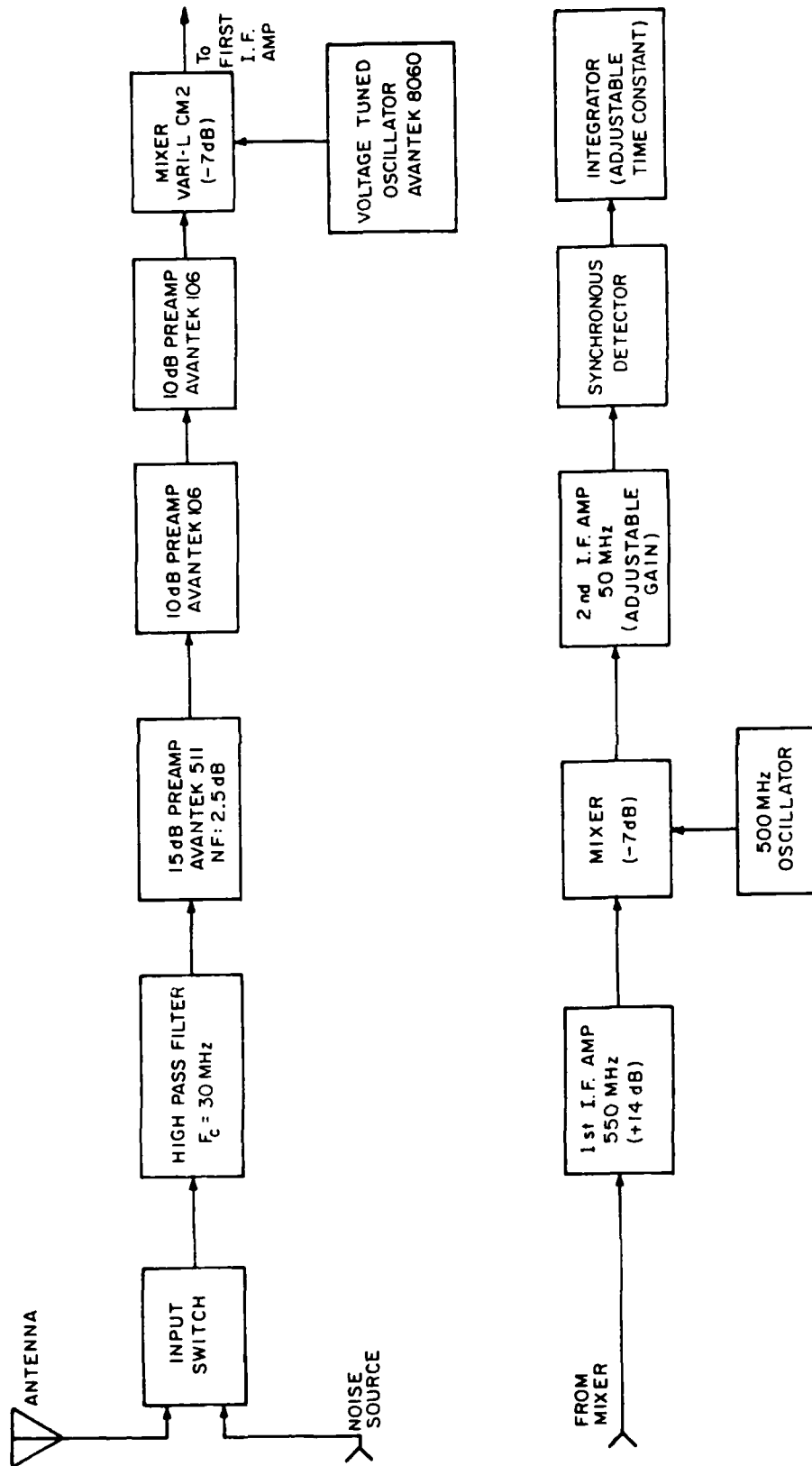


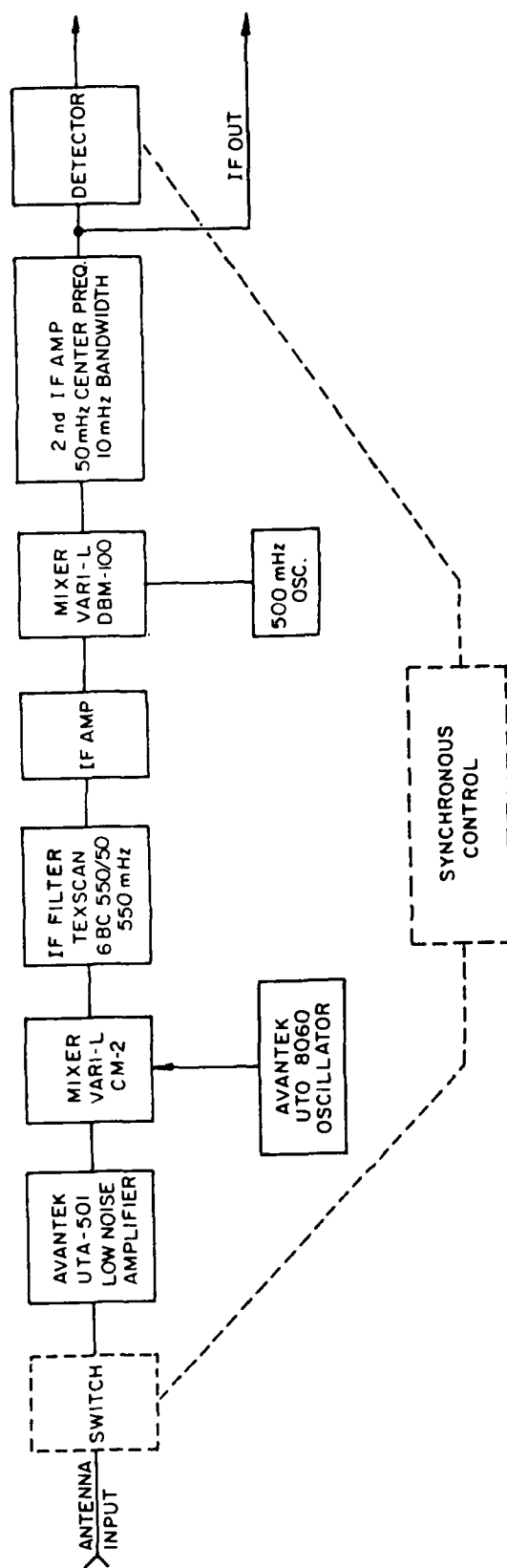
FIGURE 13. BLOCK DIAGRAM OF RADIOMETER

critical, so that any additionally required gain is easily achieved. The bandwidth of the second I.F. amplifier is 15 MHz. The output of this amplifier is detected and integrated with an adjustable integration time constant. Figure 14 is the block diagram of the receiver as finally used. It remains a straightforward double conversion design, with the input amplifier having the lowest noise figure available in a transistor amplifier. Although it was intended to be used as a high resolution integrating radiometer so that signals well below the input amplifier noise could be detected, it was found that the local man-made noise sources, generally variable in nature, could not be eliminated sufficiently to make the radiometer approach practical. This is the case since the radiometer approach works satisfactorily only when the background plus amplifier noise is reasonably constant over a period corresponding to the integration time. Accordingly the input switch was bypassed and the instrument used as a conventional wideband receiver.

2. Measurements

Figure 15 is a schematic of the typical set-up for measurement of radiation from a single rod in corona. In order to reduce background and interference, most of the measurements were made inside the metal building at the Cherry Creek Field Site.

Four different rod lengths were employed, of 0.2, 0.5, 1.0, and 2.0 meter lengths. The 0.5 and 1.0 meter rod tests were made with rods of both 1 cm and 5 cm diameter. Data were taken over the frequency range from 50 to 450 MHz. The results are shown in Figures 16-21. Each point on the graphs is an average of at least twenty individual pulses, since the corona signals, while similar in shape, varied considerably in amplitude.



RADIOMETER BLOCK DIAGRAM
FIGURE 14

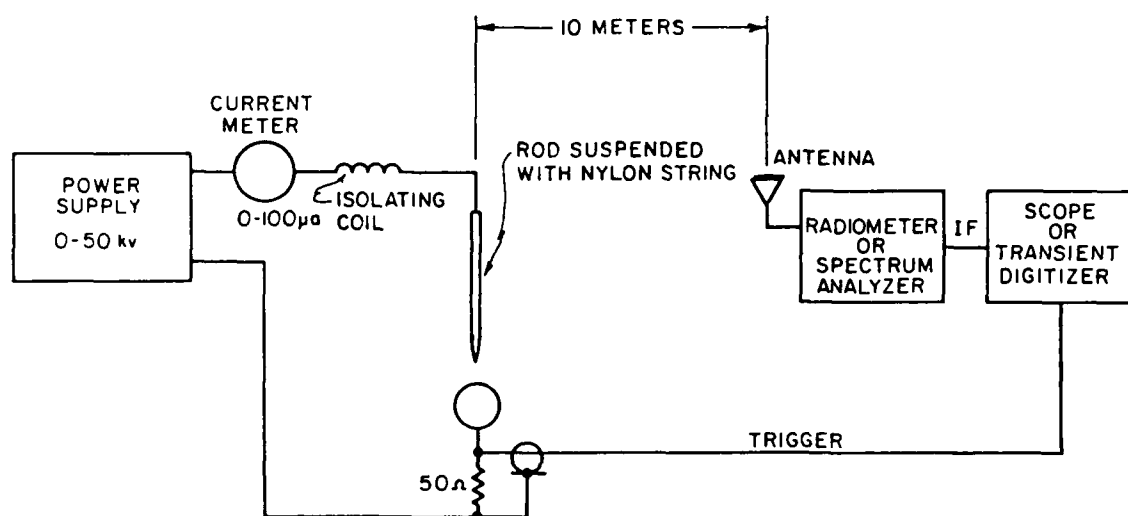


FIGURE 15

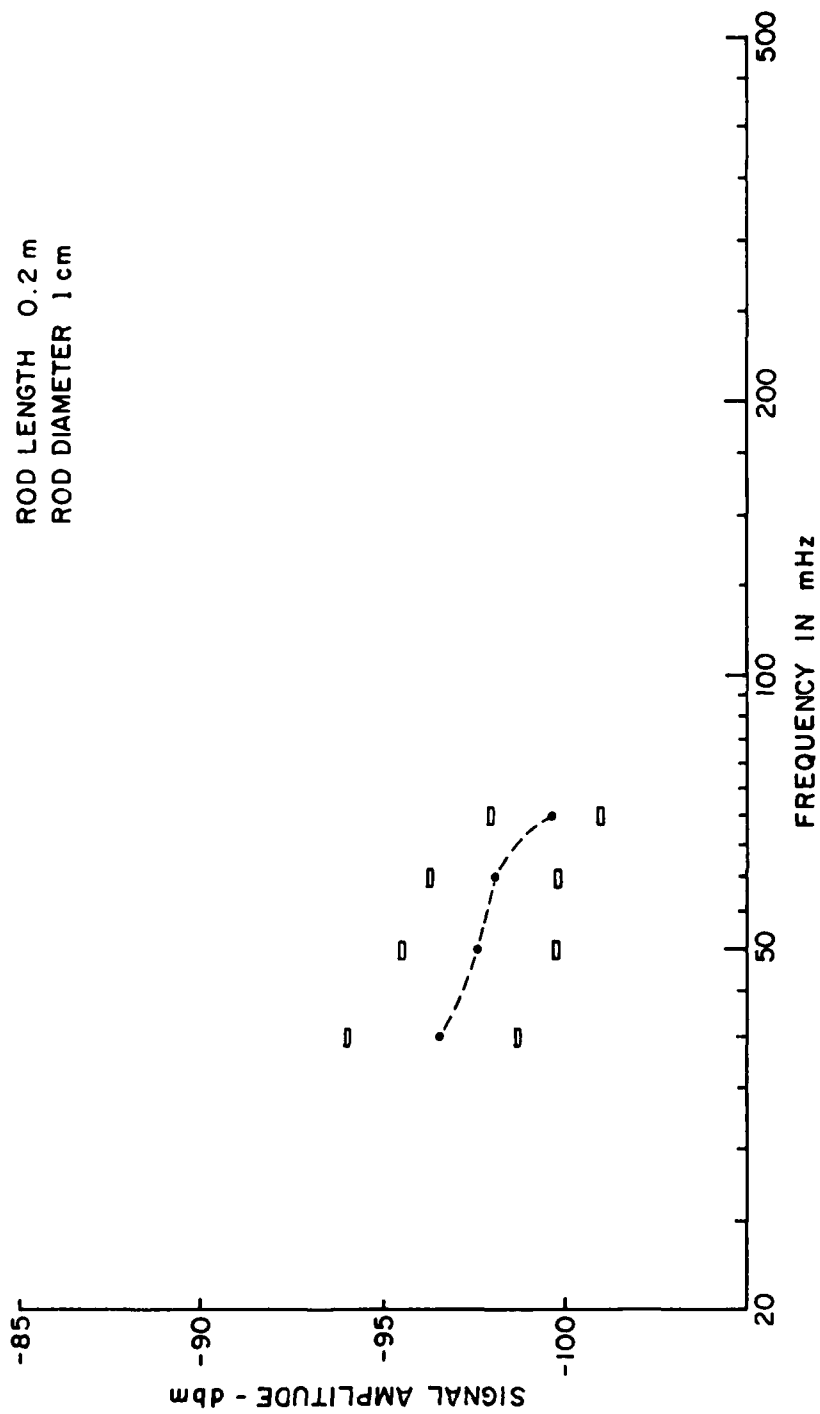


FIGURE 16

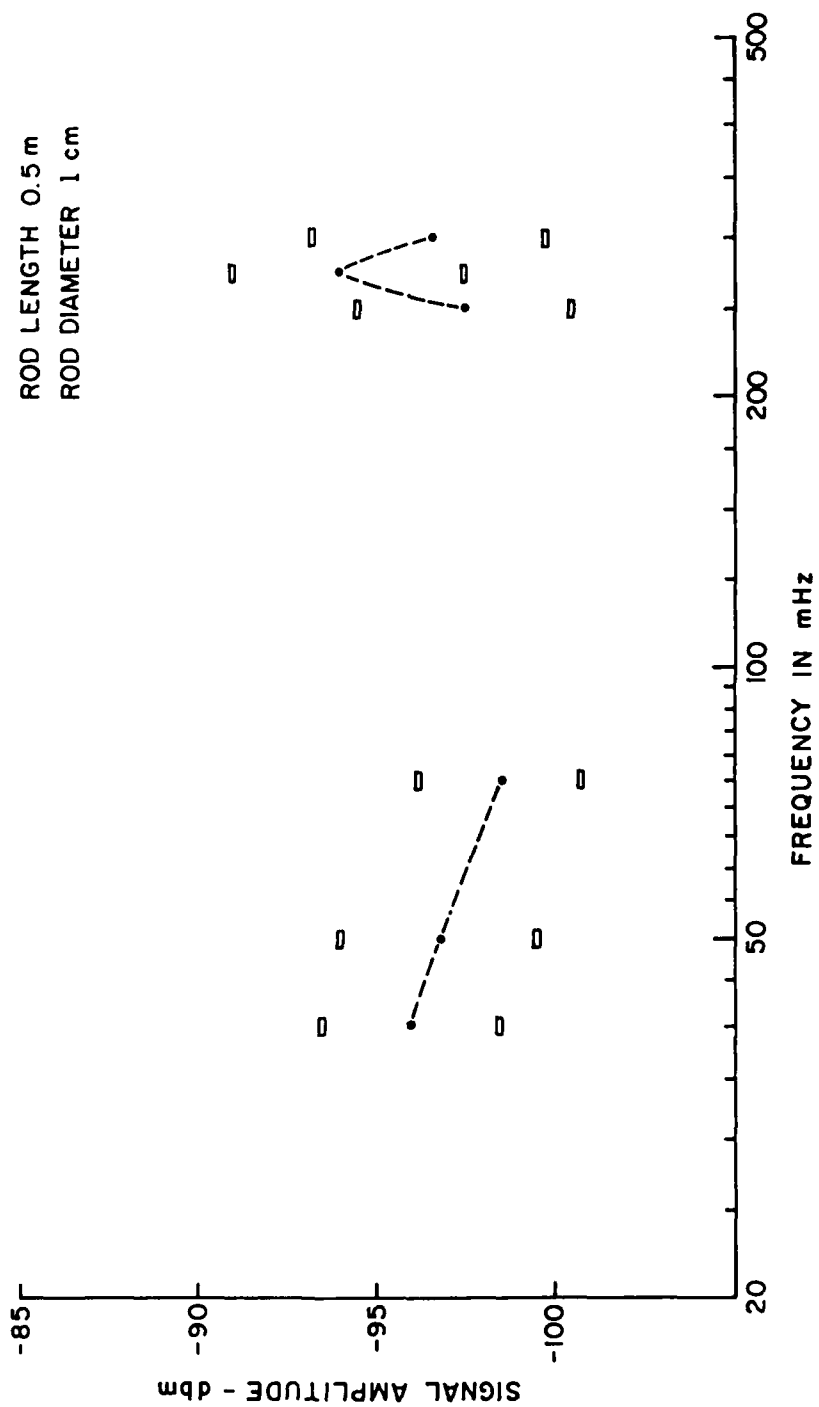


FIGURE 17

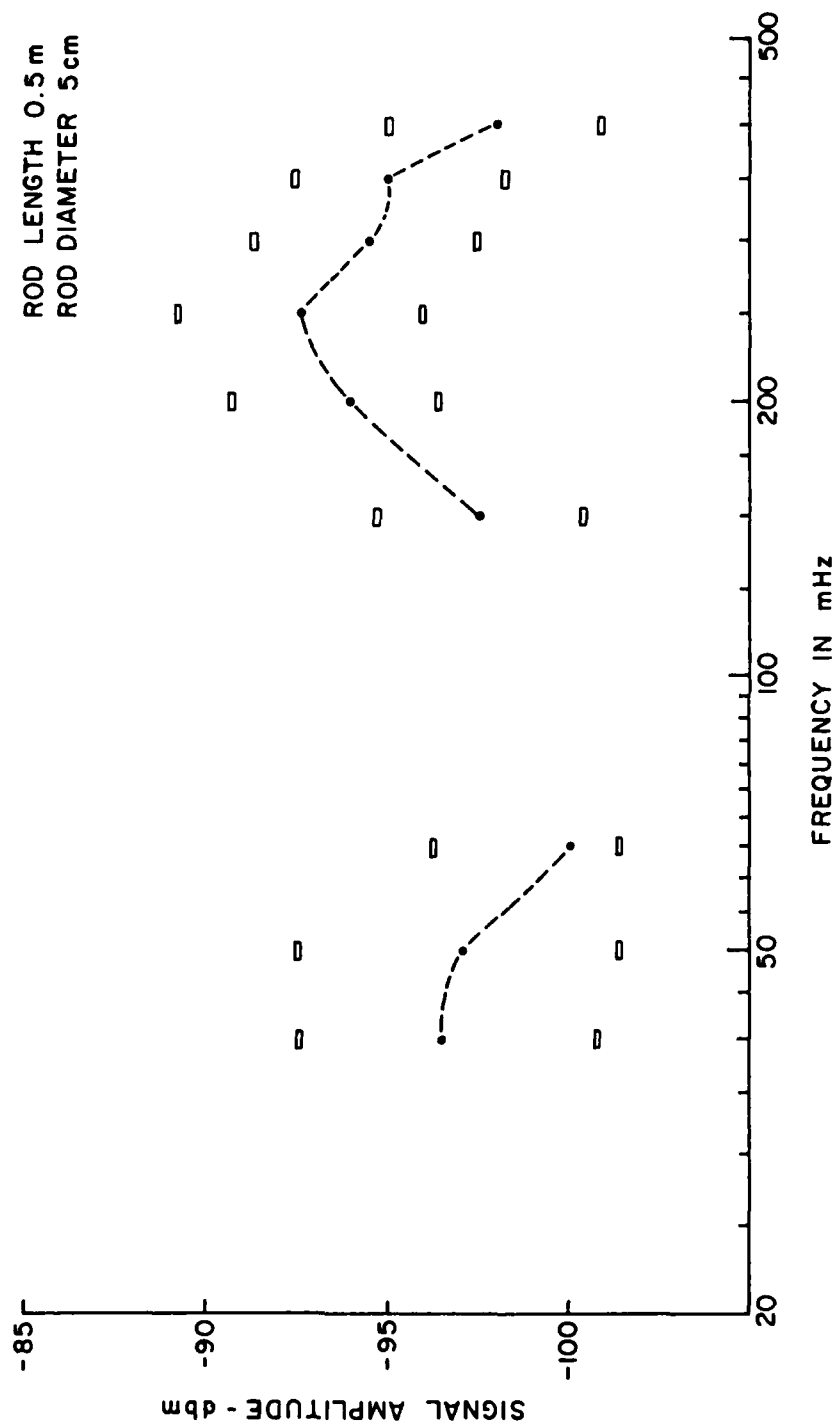


FIGURE 18

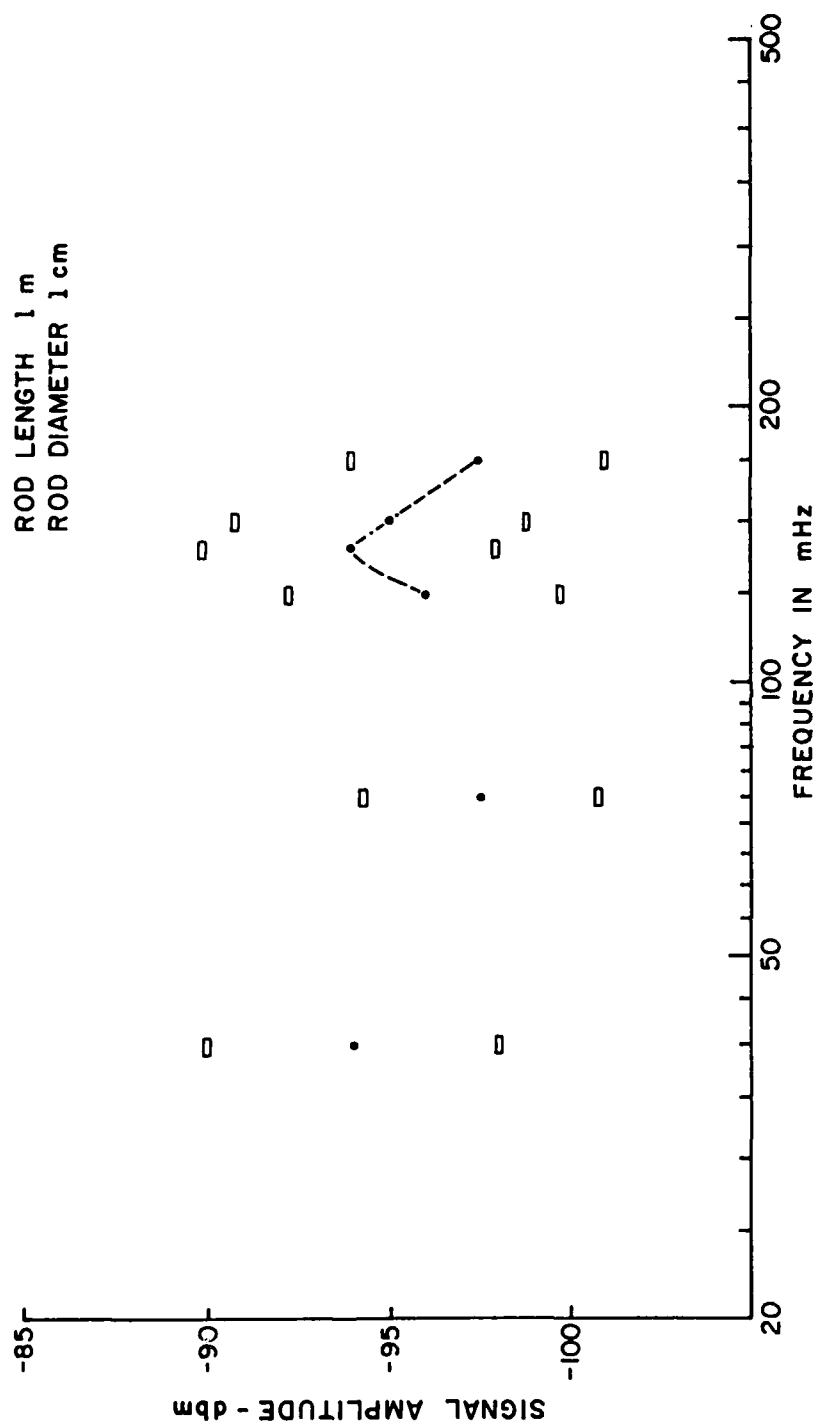


FIGURE 19

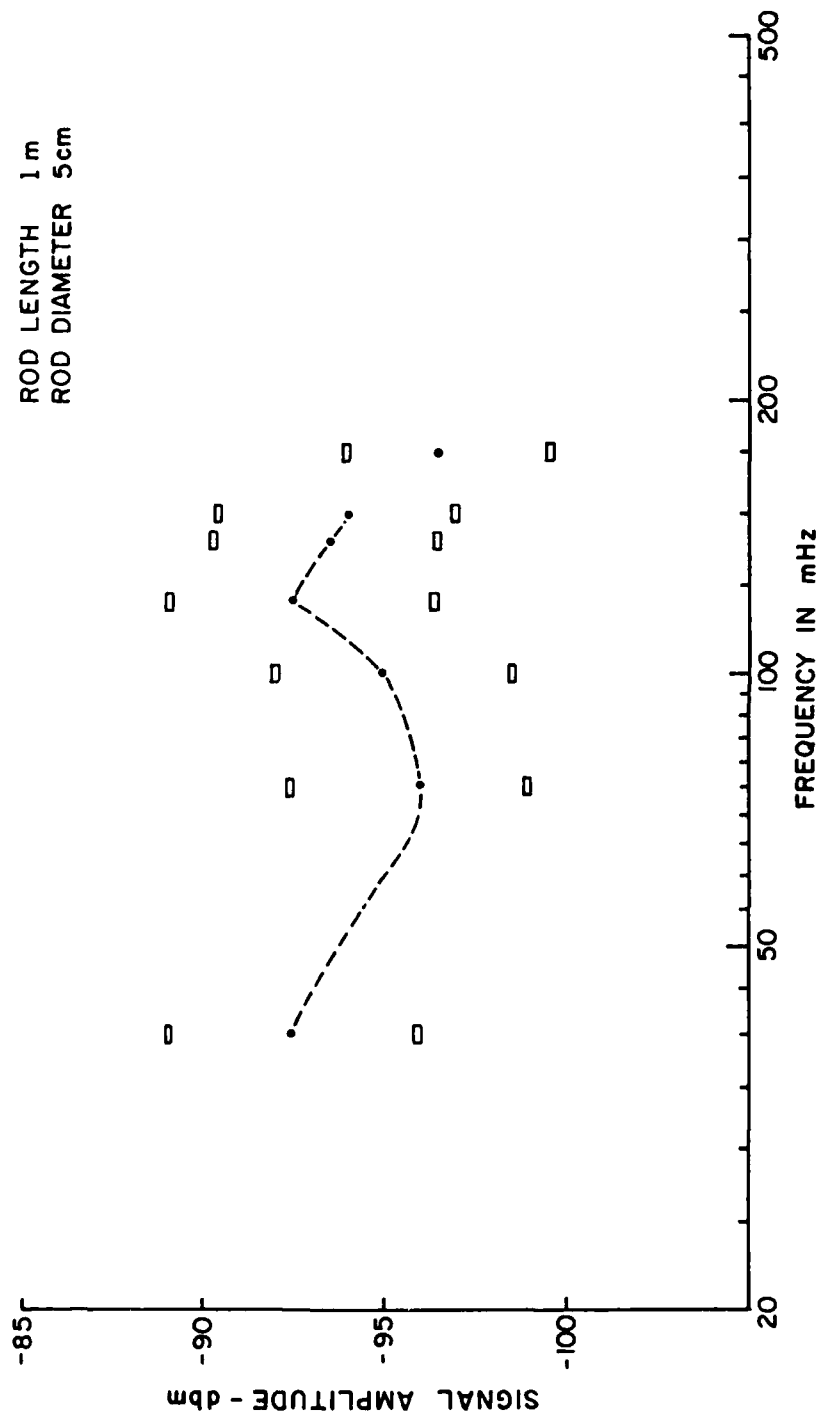


FIGURE 20

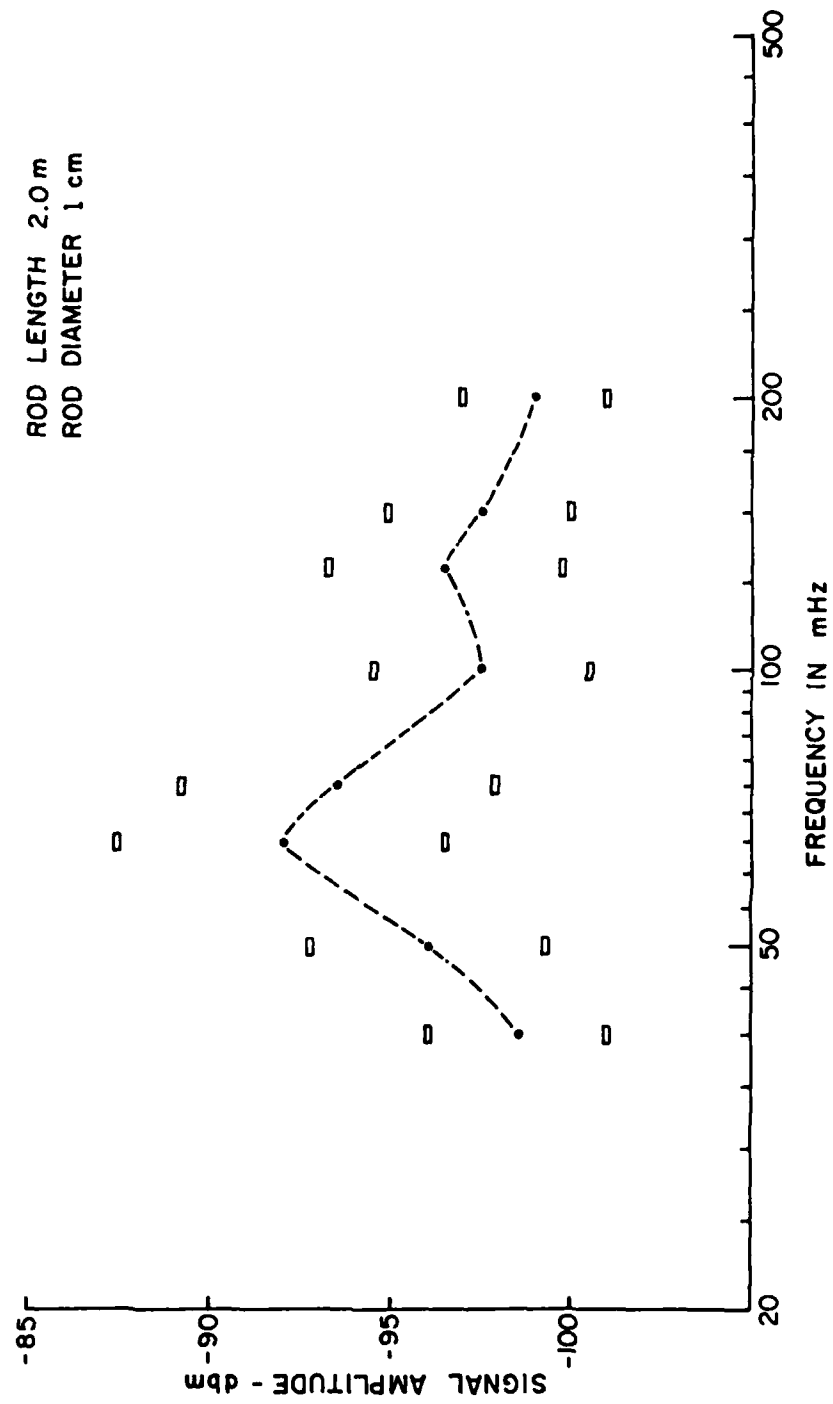


FIGURE 21

H. Model Aircraft Measurements

The conducting cylinders used in previous corona measurements were constructed of 2-1/4 inch conduit in 10 and 20 foot lengths. The length to diameter ratios were approximately 50:1 and 100:1, which were not representative of typical aircraft and missile airframes. It was decided to use a length to diameter ratio of approximately 10:1 in subsequent air frame modeling experiments. Several 5 foot sections of 8 inch and 12 inch diameter sheet metal duct pipe were obtained for this purpose. A crossed-cylinder airframe model of a KC-135 aircraft with the lengths of the wings, fuselage, and tail section scaled approximately 20:1 was then constructed. It was intended to use this model to study the radiated fields generated when several corona points were discharging at different locations along the trailing edges of the wings and tail section. It was also intended to measure the output signals with the radiometer at frequencies near the airframe resonances and in a frequency range well above the highest detected resonance. These results would then be scaled to full sized airframes and the frequency dependence of the corona signals above resonance would be determined. This information would allow calculation of the possibilities of detecting actual aircraft in corona in the presence of given average background noise conditions.

Initial tests of the radiometer indicated that its noise figure was well below the background noise in all environments available for the experiments. Figure 22 is a graph relating to receiver noise figure, where the detected output of the radiometer is plotted as a function of frequency, with -100 dbm (2.2 mv) CW signals added to the noise at 50 MHz increments. Figure 23 shows the background noise as received on the helical antenna, with the radiometer gain reduced 8 db over that in Figure 22.

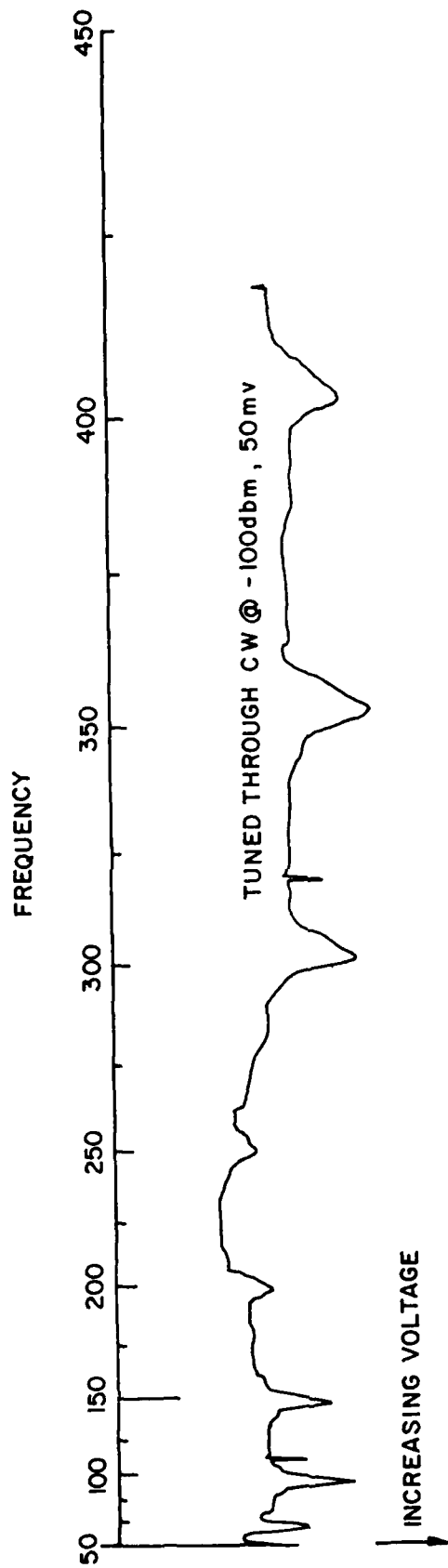


FIGURE 22
RECEIVER SENSITIVITY

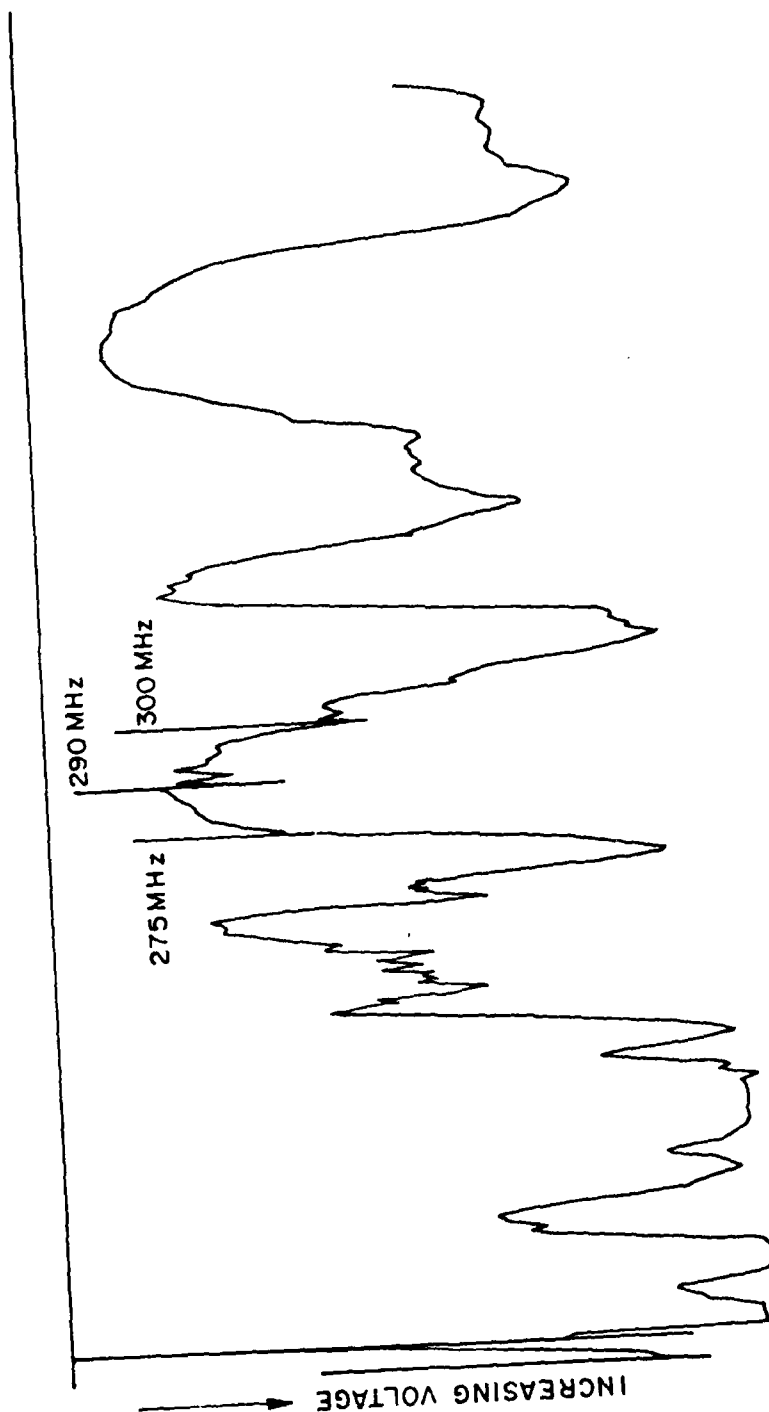


FIGURE 23
BACKGROUND NOISE

Measurements were then made of the radiation from a rod cut to resonate at 290 MHz, where the background noise is minimum, over a 15 MHz bandwidth. A diagram of the test arrangement is shown in Figure 24. Even with the antenna at a distance of 3 meters, no change could be seen in the detected output of the radiometer when the corona apparatus was activated. The corona pulses could be observed on the I.F. output of the radiometer, with a peak voltage 6 to 10 db above the average background noise.

In light of the above results, the measurements on the aircraft model were made with a log-periodic antenna and an HP8555A spectrum analyzer set to a bandwidth of 1 kHz rather than with the radiometer. Figure 25 shows the arrangement for the model aircraft tests. The resonance of the fuselage at 50 MHz is strongly apparent, with secondary resonances appearing at higher frequencies. Figure 26 shows the signal amplitude vs. frequency for a total corona current of 100 microamperes. Figure 27 shows signal amplitude vs. corona current at a frequency of 50 MHz. An attempt was then made to detect corona pulses when either of two conventional static dischargers, a wick type and a Granger null-field type, was attached to the aircraft. In both cases with discharger attached the signal was below the equipment noise level for currents up to 50 microamperes. At currents above 50 microamperes corona began to appear at points other than the dischargers and an output was again detectable.

It was apparent from these results that the frequency behavior of the corona signals above resonance could not be reliably established, and that measurements above 200 MHz were required. It was also apparent that they would have to be conducted, using the radiometer as a radiometer rather than a conventional receiver if possible, in an absolutely quiet noise environment such as a completely shielded room. Limitations of time and contract funding, however, prevented any further tests from being conducted.

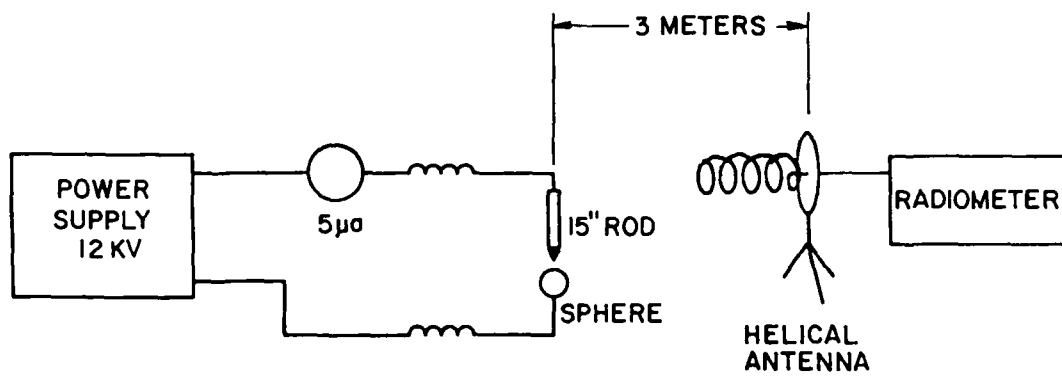


FIGURE 24

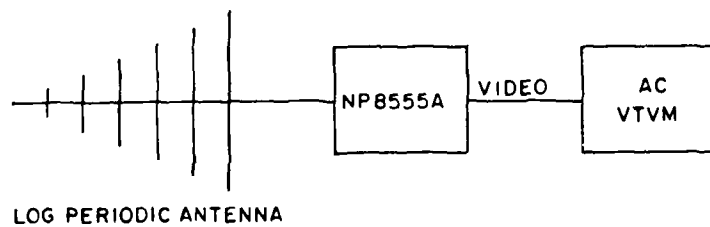
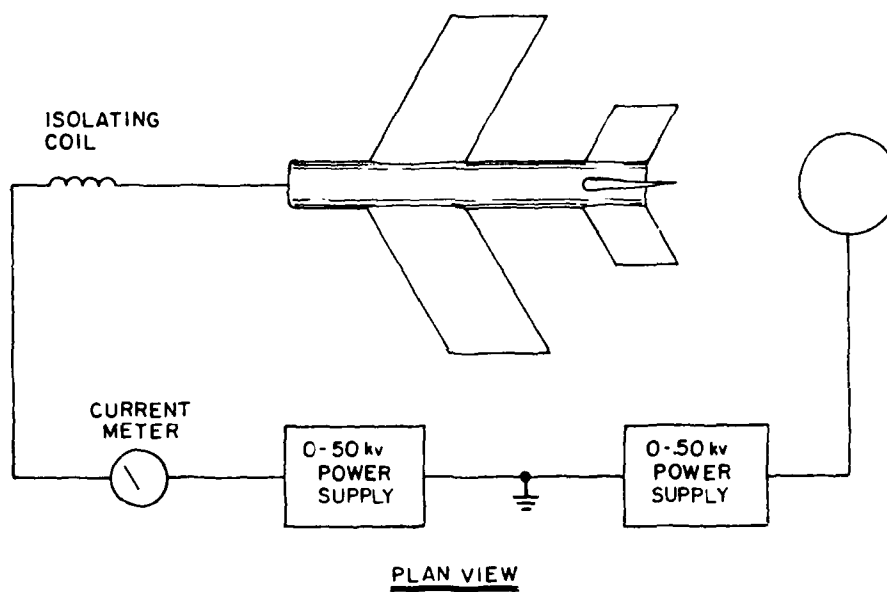
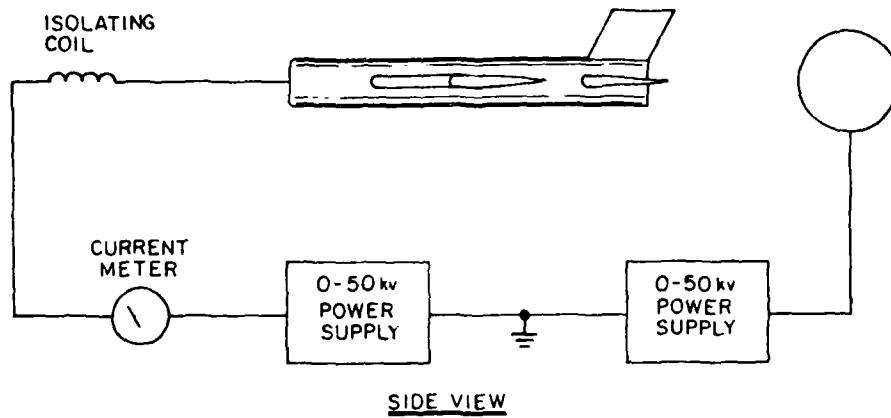


FIGURE 25

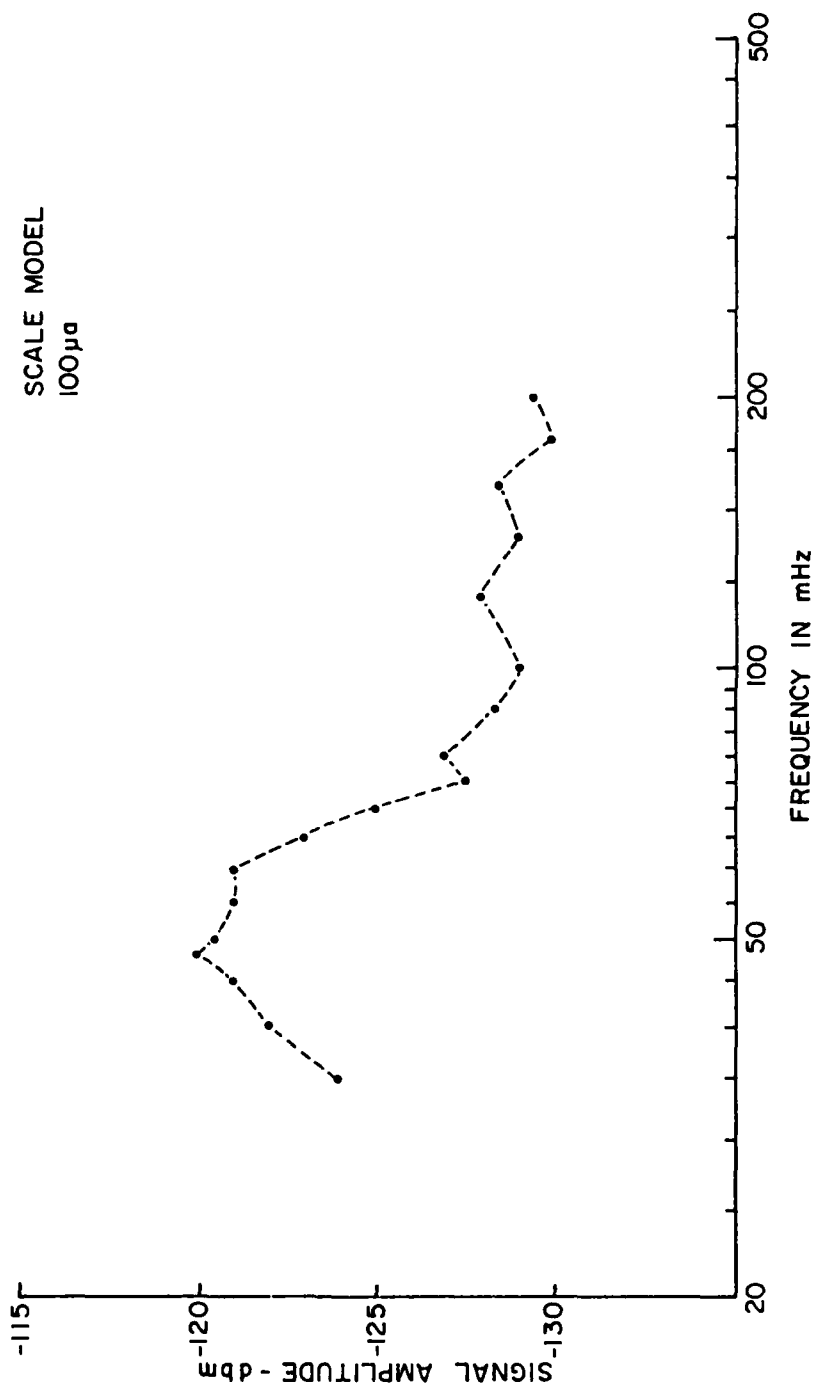


FIGURE 26

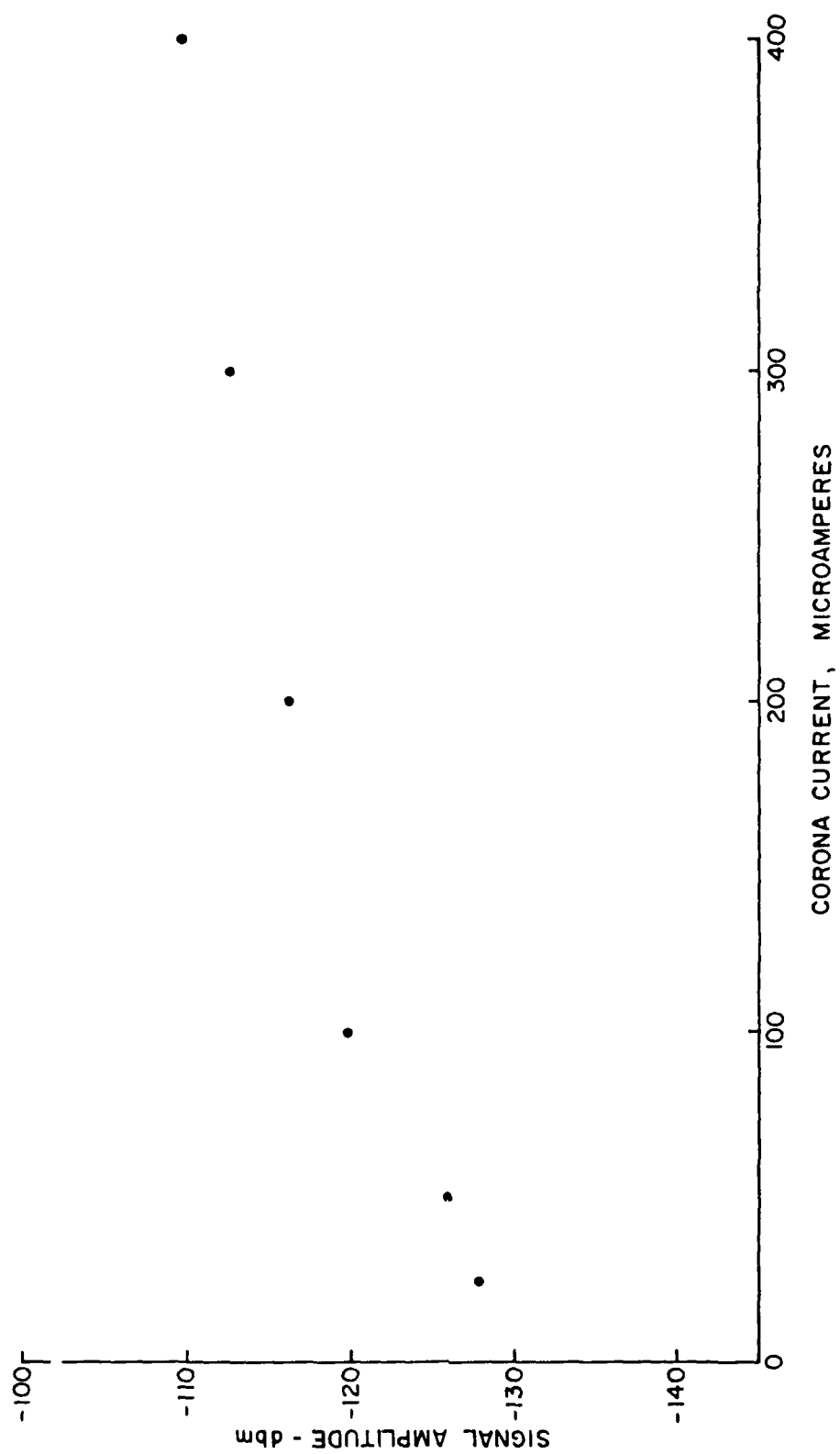


FIGURE 27

III. ANALYSIS OF RADIATED CORONA PULSE

A. The corona current in air

A corona discharge from a negatively charged conductor produces electronic and ionic currents in the air near the corona point by electron avalanching. The current is dominated initially by the motion of the electrons and later by the build up of heavy positive and negative ions. Photons emitted by the corona envelope cause further ionization of the air and also release new electrons from the conductor by photoemission. The net result is a very fast rising pulse of current during the electronic phase which decays exponentially in time during the ionic phase of the discharge. Only the electronic current component has been studied here, since it is much faster and contributes most of the high frequency content of the radiated pulse.

The electron current density in air was calculated by solving Townsend's equations for an electron in a non-uniform electric field between a negatively charged point and a grounded plane.⁽²⁾

The result is given by the equation

$$J(x', t') = qn_0 \delta(t' - \tau) \exp \left\{ (Ap/C_1) \left[1 - \exp(-C_1 X') \right] \exp(-C_1 a) \right\} \quad 3.1$$

where

q = electron charge (1.602×10^{-19} coulombs)

n_0 = number density of initial electrons (electrons/cm²)

A = constant (14.6)

p = atmospheric pressure (760 mm)

C_1 = constant (160)

a = radius of corona point (0.01 cm)

The parameter τ was determined from the differential equation for the electron velocity and from the mobility equation, which relates the velocity to the electric field. The solution gives

$$\tau = \frac{C_1(2ax' + x'^2)}{2Bpb} \quad 3.2$$

where

b = electron mobility (500 cm/sec per volt/cm),

B = constant (365).

B. The corona current on a conducting cylinder

The pulse of current launched onto a conductor when a corona discharge occurs can be determined by equating the work done by the field to the change in energy of the charged conductor. This gives

$$i(t') = \frac{1}{V} \int E(x') J_1(x', t') d^3x' \quad 3.3$$

where $i(t')$ is the current pulse on the conductor. This equation was evaluated by substituting equation 3.1 for J_1 and approximating the field distribution by the equation

$$E(x') = \frac{V}{(a+x') \ln(2l/a)} \quad 3.4$$

which is a sufficient approximation for the field between a point of radius "a" raised to a potential V and a plane at a distance l from the point. (3)

With these substitutions the integral in equation 3.3 evaluates to

$$i(t') = \frac{i_0 \exp \left\{ (Ap/C_1) \left[1 - \exp(-C_1 \sqrt{a^2 + 2Bpb t'/C_1} - a) \exp(-C_1 a) \right] \right\}}{a^2 + 2Bpb t'/C_1} \quad 3.5$$

where

$$i_0 = \frac{\pi d^2 q n_0 Bpb}{C_1 \ln(2l/a)} \quad 3.6$$

The corona channel was assumed to be cylindrical of radius d (cm) in this derivation. The current pulse given by equation 3.5 is shown plotted in

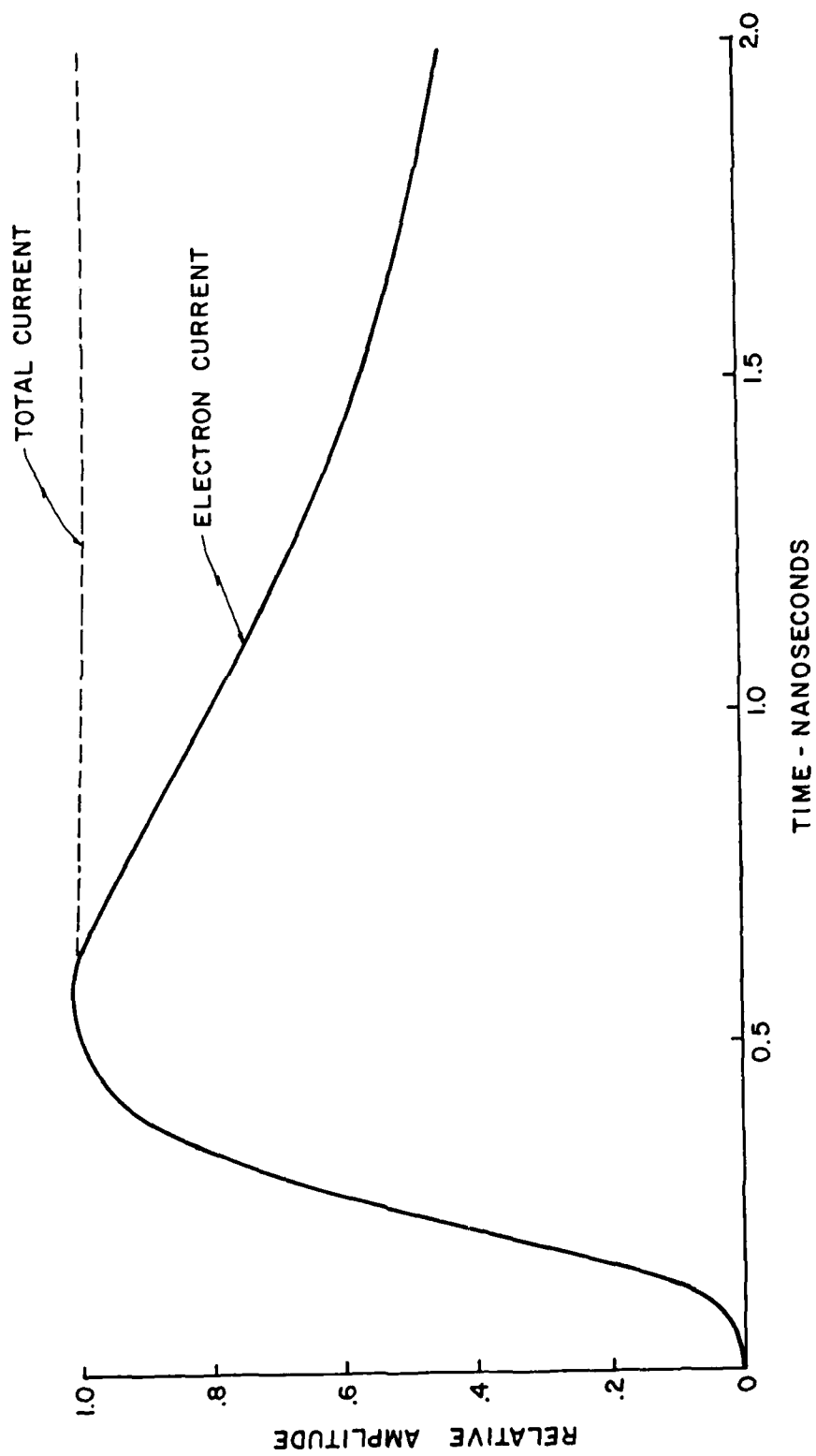


FIGURE 28. CALCULATED CURRENT PULSE ON A CYLINDER

Figure 28 using appropriate values for the various constants in equations 3.5 and 3.6, consistent with a typical discharge.⁽⁴⁾

C. The radiated fields

The fields radiated by the corona current in air, and the current on the cylinder have been calculated separately by evaluating the vector potential for each case. The vector potential is given by the equation⁽⁵⁾

$$A_{1,2}(r,t) = \frac{1}{c} \int d^3x' \int dt' \left\{ \frac{J_{1,2}(x',t') \delta(t' + r/c - t)}{r} \right\} \quad 3.7$$

where the subscript 1 applies to the corona current in air and the subscript 2 applies to the current on the cylinder. The constant c is the speed of light and the primed and unprimed variables refer to the source and receiver coordinates respectively. The distance r is measured from the current element $J(x',t')$ to the receiving point. The geometry is shown in Figure 29.

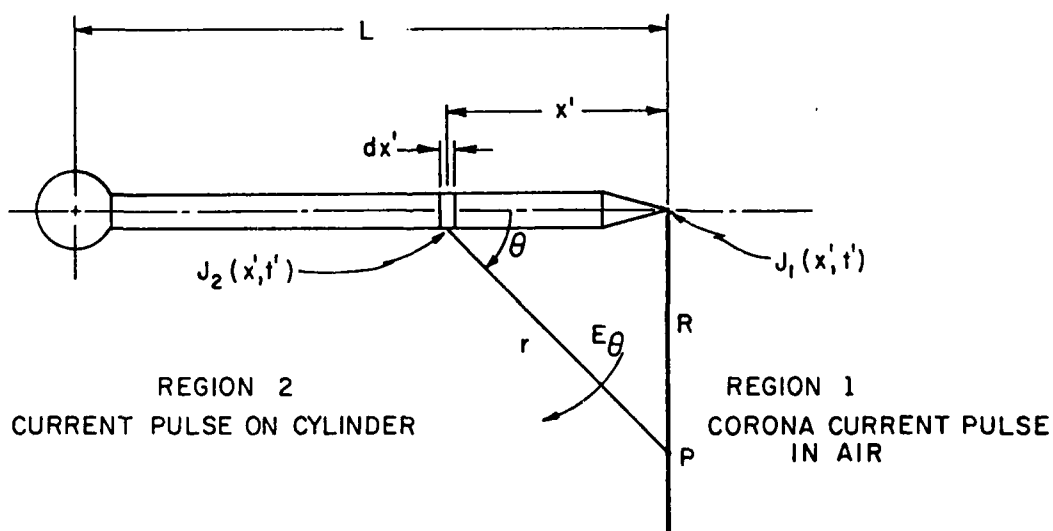


Figure 29. Source Geometry

The electric field component E_θ in the radiation zone is related to the vector potential by the equation

$$E_\theta = -\frac{1}{c} \frac{\partial A}{\partial t} \quad 3.8$$

and the magnetic field H_ϕ is then given by $H_\phi = E_\theta / (120\pi)$. 3.9

The integration of equation 3.7 was carried out directly in the time domain in region 1, using equation 3.1 for J_1 . The final result can be written in the form

$$e_1(t) = \frac{m C_3 \exp \left\{ C_2 \exp (-C_1 \sqrt{a^2 + mt}) \right\}}{2 c^2 R (a^2 + mt)} \quad 3.10$$

$$\left\{ C_1 C_2 \exp (-C_1 \sqrt{a^2 + mt}) + \frac{1}{\sqrt{a^2 + mt}} \right\} \sin \theta$$

where $m = 2 Bpb/C_1$ 3.11

$$C_2 = -Ap/C_1 \quad 3.12$$

$$C_3 = n_0 \pi d^2 q m \exp \left[-C_2 \exp (-C_1 a) \right] / 2 \quad 3.13$$

and the approximations

$$r \simeq R (1 - x' \cos \theta / R) \quad 3.14$$

$$d^3 x' \simeq \pi d^2 dx' \quad 3.15$$

$$x/R \ll 1 \quad 3.16$$

have been used. Equation 3.10, which gives the electric field pulse radiated by the corona current in air is shown plotted in Figure 30.

The fields radiated by the current on the cylinder in region 2 were computed in the frequency domain and then transformed back into the time domain. For this case the vector potential has the form

$$A(R, \omega) = \frac{K(\omega) \exp(-ikR) \int dx' I(x') \exp(-ikx' \cos \theta)}{CR} \quad 3.17$$

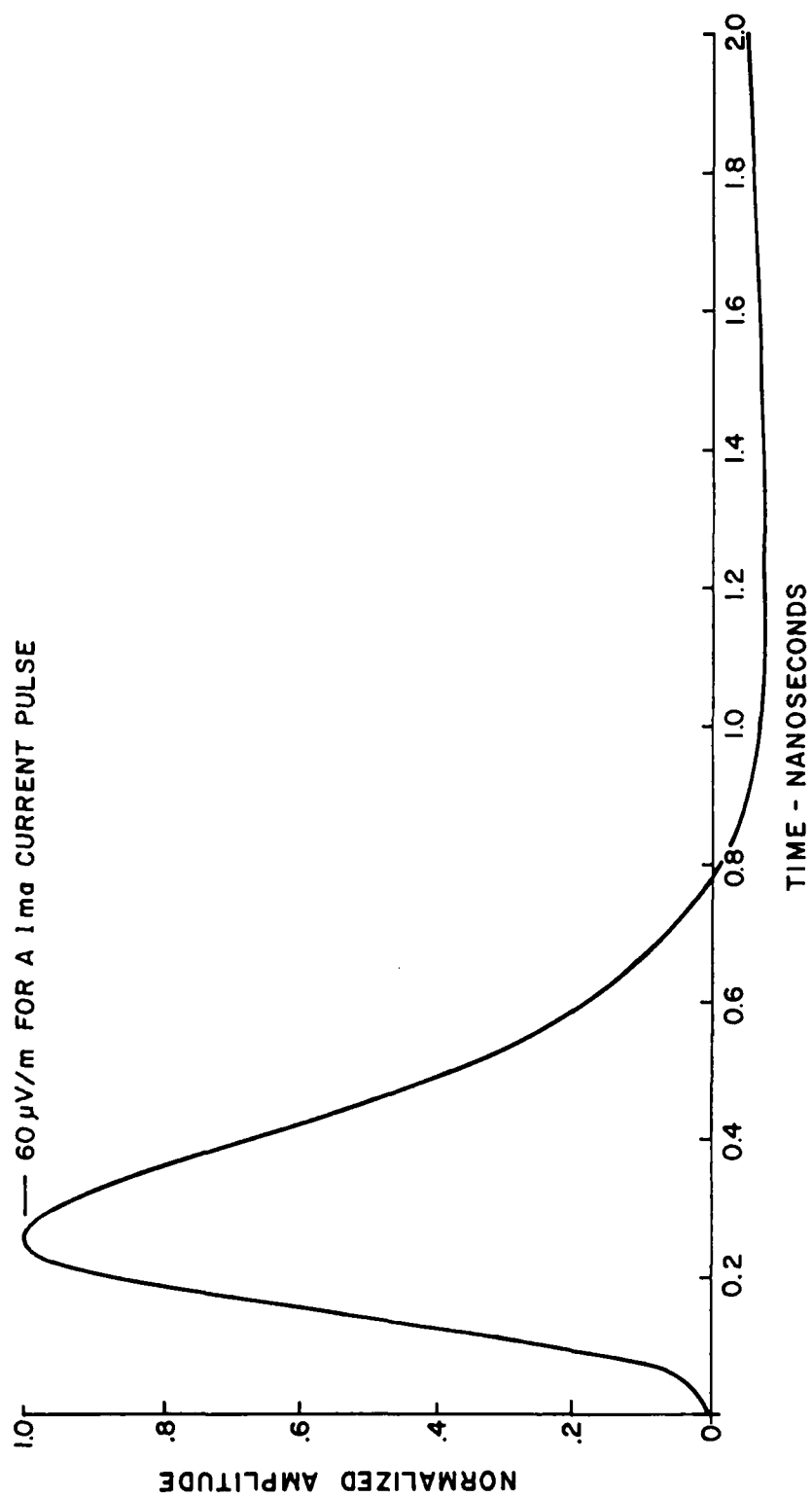


FIGURE 30. RADIATED PULSE FROM CORONA ELECTRON CURRENT IN AIR

where $K(\omega)$ is the spectrum of the current pulse defined by equation 3.5 and plotted in the time domain in Figure 28.

$I(x')$ is the current distribution along the cylinder and $k = \omega/c$ is the propagation constant in free space. $I(x')$ can be determined from transmission line theory, which for a thin cylinder has the form⁽⁶⁾

$$\begin{aligned} I(x') = & \exp(-\gamma x') + T_1 \exp[-\gamma(2L-x')] + T_0 T_1 \exp[-\gamma(2L+x')] \\ & + T_0 T_1^2 \exp[-\gamma(4L-x')] + T_0^2 T_1^2 \exp[-\gamma(4L+x')] \\ & + T_0^2 T_1^3 \exp[-\gamma(6L-x')] + \dots \end{aligned} \quad 3.18$$

The substitution of equation 3.18 into 3.17 and evaluation of the integral gives the vector potential in region 2. The radiated electric field at point P is then determined from equation 3.8. The result is

$$\begin{aligned} E(R, \omega) = & \frac{L \sin \theta}{2Rc^2} \exp(-ikR)(i\omega) K(\omega) \left\{ \frac{\sin kz_1}{kz_1} \left[\exp(-ikz_1) \right. \right. \\ & + T_0 T_1 \exp(-ik(2L+z_1)) + \dots \left. \right] \\ & + \frac{\sin kz_2}{kz_2} \left[T_1 \exp(ik(2L-z_2)) + T_0 T_1^2 \exp(-ik(4L-z_2)) + \dots \right] \left. \right\} \end{aligned} \quad 3.19$$

The above results pertain to a cylinder of length L where T_0 is the reflection coefficient at the corona end of the cylinder and T_1 is the reflection coefficient at the opposite (open) end. γ is the transmission constant given by

$$\gamma = \alpha + ik \quad 3.20$$

where α gives the attenuation and k is the phase constant of the cylinder when treated as a transmission line. The variables Z_1 and Z_2 are defined by the equation

$$Z_{1,2} = L(1 \pm \cos \theta)/2 \quad 3.21$$

For the special case $\theta = \pi/2$, $Z_1 = Z_2 = L/2$ and equation 3.19 can be written in MKS units as

$$E(R, \omega) = \frac{30K(\omega)}{R} (\sin \pi L/\lambda) \left\{ \exp \left[-ik(R+L/2) \right] + \dots \right\} \quad 3.22$$

where the terms in braces correspond to the successive reflections from the two open ends of the cylinder.

The inverse transform of equation 3.19 gives the time domain solution. This is most easily obtained by using the time convolution theorem for the products of frequency functions, which has the notation

$$f_1(t) * f_2(t) * \dots \longleftrightarrow F_1(\omega) \cdot F_2(\omega) \cdot \dots \quad 3.23$$

where the asterisk denotes convolution and the arrow signifies the Fourier transform. The final result in MKS units can be written

$$\begin{aligned} e(R, t) = \frac{15}{R} i(t) * \left\{ \frac{\sin \theta}{1 + \cos \theta} \left[\delta(t^*) - \delta(t^* - 2Z_1/C) + T_0 T_1 \delta(t^* - 2L/C) \right. \right. \\ \left. \left. - T_0 T_1 \delta(t^* - 2L/C - 2Z_1/C) + \dots \right] \right. \\ \left. + \frac{\sin \theta}{1 - \cos \theta} \left[T_1 \delta(t^* - 2L/C + 2Z_2/C) - T_1 \delta(t^* - 2L/C) + \dots \right] \right\} \end{aligned} \quad 3.24$$

where $t^* = t - R/C$.

The reflection coefficients T_0 and T_1 have been assumed independent of frequency in equation 3.24, so that only the amplitude and not the shape of the current pulse $i(t)$ is changed upon reflection.

The form of equation 3.24 is convenient for computations because the convolution of the current pulse $i(t)$ with the string of delta functions contained within the braces simply superimposes the pulses, each shifted in time to that given by the argument of each delta function. The results for the special case $\theta = \pi/2$ and $T_0 = T_1 = -0.8$ are depicted diagrammatically in Figure 31.

All of the calculations have been carried out for a conductor in free (air) space. The results for a conductor near the earth would be modified by the image currents in the ground. The effect on the radiated signal from a vertical conductor over ground of finite conductivity would be to increase the signal amplitude by the factor $(1+R)$, where R is the ground reflection coefficient, which is positive for vertical polarization. For infinite conductivity, $R = +1$ and the signal amplitude would be doubled.

The horizontally polarized field radiated by an elevated conductor mounted parallel to the earth's surface can also be estimated. For this case the ground reflection coefficient is approximately equal to -1 for all frequencies. The resultant field at an elevated receiving antenna, which is the sum of a direct and a ground reflected component, would be proportional to the derivative of the free space field over a restricted frequency range. This can be seen from the equation

$$E(t) = e(t) + Re(t - \tau) \quad 3.25$$

where

$e(t)$ is the free space field,

R is the reflection coefficient for horizontal polarization ($R = -1$),

τ is the path difference delay time.

$E(t)$ is the resultant field at the antenna.

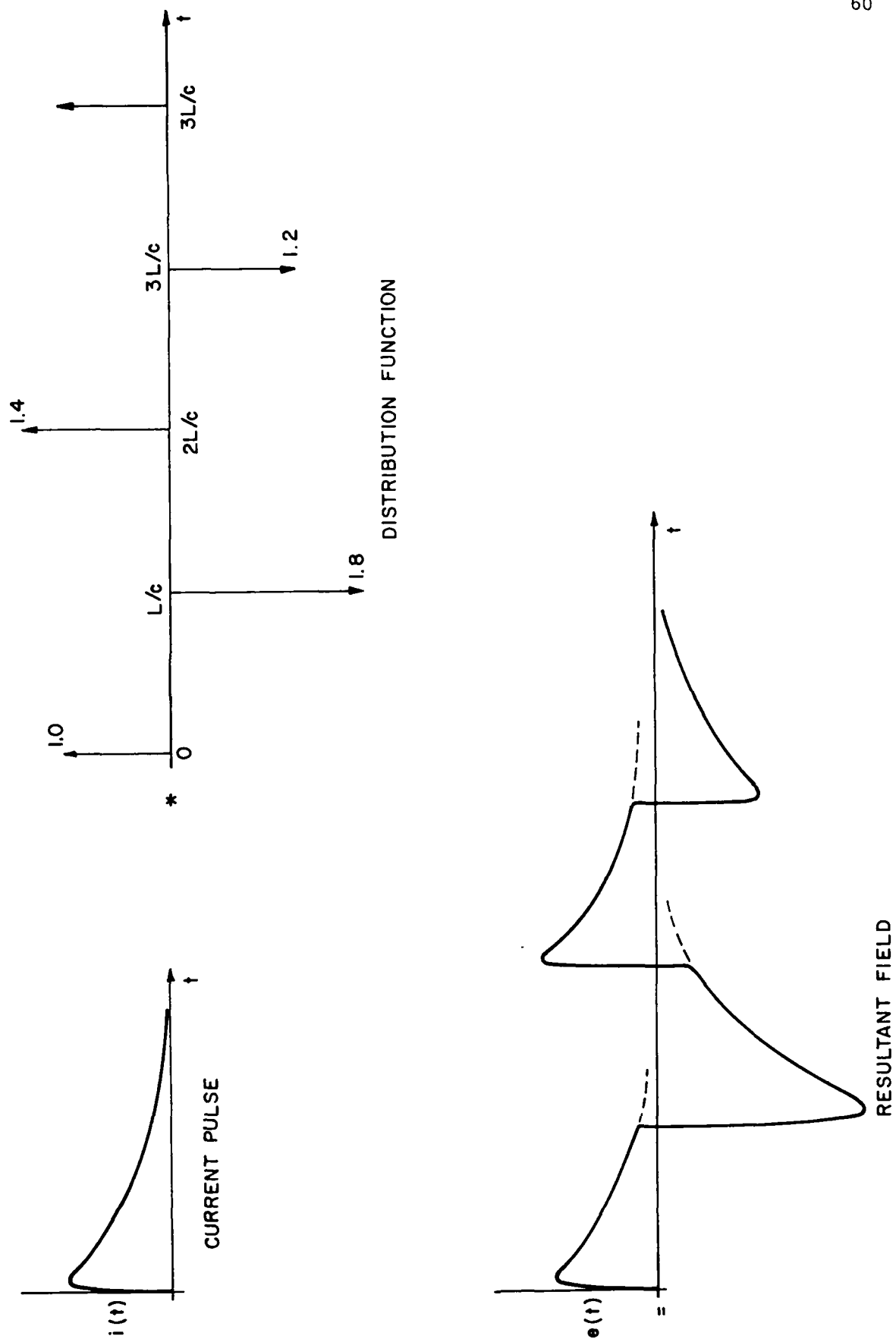


FIGURE 31. SYNTHESIS OF THE RADIATED PULSE TRAIN BY CONVOLUTION

The substitution $t' = t + \tau/2$ and $R = -1$ gives

$$E(t') = e(t' + \tau/2) - e(t' - \tau/2) \quad 3.26$$

which has the Fourier transform

$$G(\omega) = i\omega\tau F(\omega) \frac{\sin(\omega\tau/2)}{\omega\tau/2} \quad 3.27$$

where $G(\omega)$ is the Fourier transform of $E(t)$ and $F(\omega)$ is the Fourier transform of $e(t)$. When $\omega\tau$ is small,

$$G(\omega) \simeq i\omega\tau F(\omega) \quad 3.28$$

which transforms back into the time domain as

$$E(t) \simeq \tau \frac{de(t)}{dt} \quad 3.29$$

This shows that the resultant horizontal field at the antenna is approximately proportional to the derivative of the free space field. The frequency range over which 3.27 is valid is determined by the sinc function. Thus for 10% accuracy the requirement is

$$0.9 \leq \sin c(\omega\tau/2) \leq 1 \quad 3.30$$

which is met when $f\tau \leq 0.25$. As an example, if the time difference τ was 5 nanoseconds, the resultant field would be proportional to the derivative (within 10%) for frequencies

$$f \leq 0.25/(5 \times 10^{-9}),$$

or

$$f \leq 50 \text{ MHz.}$$

An order of magnitude estimate of the radiated spectral amplitude $E(R, \omega)$ can be obtained from equation 3.22 once the spectrum $K(\omega)$ of the current pulse is known. This could be computed numerically from the recorded corona current pulse shown in Figure 6; however, for the frequency range of

interest, the pulse is adequately represented in closed form by the double exponential function

$$i(t) = i_0 \left[\exp(-at) - \exp(-bt) \right] \quad 3.31$$

which has the Fourier transform

$$K(\omega) = \frac{i_0}{a - \omega^2/b - i\omega} \quad 3.32$$

where i_0 is the peak amplitude of the current pulse and the decay constants a and b have the values

$$a = 3.3 \times 10^7, \quad b = 9.4 \times 10^9. \quad \text{With } i_0 = 5 \text{ ma, } f = 50 \text{ MHz,}$$

the magnitude of the spectrum is

$$|K(f)| = 1.6 \times 10^{-11} \text{ amp-sec} \quad 3.33$$

Substitution of this value into equation 3.22 gives

$$E(f) = 2 \times 10^{-9} \text{ v-sec/m at 1 meter for a single pulse train}$$

radiated by a cylinder of length $L = 10$ feet.

IV. THEORETICAL DISTANCES FOR CORONA DETECTION

It is possible to develop an analytic expression for the power available from an incident field at the input to a narrow-band receiving device in the following way: an instrument such as the H-P spectrum analyzer measures the power

$$\begin{aligned}
 P &= R i_{\text{eff}}^2 \\
 i_{\text{eff}} &= \frac{v_{\text{eff}}}{R} \\
 P &= \frac{R v_{\text{eff}}^2}{R^2} = \frac{v_{\text{eff}}^2}{R} \\
 v_{\text{eff}} &= \frac{v_p}{\sqrt{2}}
 \end{aligned}$$

Therefore $P = \frac{v_p^2}{2R}$

where v_p is the peak voltage output of the narrow-band filter. If B is the bandwidth of the idealized filter, and F_s (volt-seconds) is the spectral amplitude of the input to the filter, then the output voltage of the filter can be shown to be

$$v_p = \frac{B}{2} F_s \text{ volts}$$

and the power is

$$P = \frac{B^2 F_s^2}{4 \times 2R}$$

If the voltage gain of the system is g_s , then in terms of the voltage at the antenna load, F_a

$$F_s = g_s F_a$$

and

$$P = \frac{B^2 g_s^2 F_a^2}{8R}$$

The antenna circuit may be approximated by the antenna radiation resistance R_a in series with the load resistance R , with the voltage F_a appearing across R , so that

$$F_a = F_i \frac{R}{R_a + R}$$

and

$$P = \frac{g_s^2 B^2}{8R} \left(\frac{R}{R_a + R} \right)^2 F_i^2$$

But $F_i = E_i h_e$

where E_i is the incident field spectral amplitude in volt-seconds/meter and h_e is the antenna effective height.

Therefore

$$P = \frac{g_s^2 B^2}{8R} \left(\frac{R}{R_a + R} \right)^2 h_e^2 E_i^2$$

In terms of antenna parameters and wavelength the effective height of any antenna is

$$h_e = \frac{\sqrt{R_a g_a} \lambda}{\sqrt{120 \pi}} \text{ meters}$$

where R_a = antenna radiation resistance and g_a = antenna gain.

Therefore

$$P = \frac{g_s^2 B^2}{8R} \left(\frac{R}{R_a + R} \right)^2 \frac{R_a g_a \lambda^2}{120 \pi^2} E_i^2$$

But $c = f\lambda$ in free space, and

$$P = \left[\frac{g_s^2}{8R} \left(\frac{R}{R_a + R} \right)^2 \frac{c^2 R_a g_a}{120 \pi^2} \right] \left(\frac{B}{f} \right)^2 E_i^2$$

For a given antenna system and load the bracketed term is some constant K, and

$$P = K \left(\frac{B}{f} \right)^2 E_i^2$$

The constant K, which is a property of the propagation medium and the receiving antenna and associated system, is easily determinable. However, the incident field arising from the radiation caused by a corona discharge is not. The coupling established between the corona discharge current in an airframe and the on-board antenna systems has been extensively studied.* But the behavior of the corona current acting as a radiating system into free space is not well understood, and it was beyond the scope of this project to undertake such a theoretical analysis in any but the simplest geometries.

However, based on purely power considerations and in accordance with the analysis above, it is possible to estimate an upper bound on the distances at which a narrow-band receiver, operating at a given frequency and with a given bandwidth and noise figure, might be expected to be able to sense a corona pulse.

For example, if the corona pulse is idealized to a current step of 10 ma, and the transmitting and receiving systems are assumed to be matched at 75 ohms, with a 1 MHz bandwidth and operating at 300 MHz, then the power dissipated in a 75 ohm resistor would be

$$P = \frac{(0.01)^2}{2} \left(\frac{1}{300} \right)^2 (75) = 4.17 \times 10^{-8} \text{ watts}$$

If this power were all radiated uniformly then the power density at one meter would be

$$P_d = \frac{4.17 \times 10^{-8}}{4\pi(1)^2} = 0.332 \times 10^{-8} \text{ w/m}^2$$

*Vassiliadis, "A Study of Corona Discharge Noise in Aircraft Antennas," SRI Report #70 on Contract AF19(604)-3458, August, 1960.

Now assume a receiving antenna with a radiation resistance of 75 ohms and an effective area of 1 m^2 (antenna gain = 11 db). Also assume that it has a noise figure of 4 db, which corresponds to a power of 10^{-14} watts. Then the distance at which the received power equals the receiver noise is found from

$$\frac{4.17 \times 10^{-8}}{4\pi d^2} = 10^{-14}$$

or $d = 576$ meters.

If the received pulse width from the 1 MHz bandwidth receiver is assumed to be 1 microsecond, and if the pulse repetition rate is 50 kHz, then a similar calculation shows that the distance at which the average radiated power is equal to the receiver noise is 125 meters.

The theory shows that this situation can be improved considerably by employing wider bandwidths and operating at lower frequencies, since the received power is proportional to $\left(\frac{B^2}{F}\right)$. Also, on an actual aircraft in corona there would probably be many corona points so that the peak power might be expected to increase substantially at random times as multiple corona points radiate coherently. However, those experiments which have been conducted indicate great difficulty in locating physical areas where the natural background noise is at or below the noise figure of a good receiver, and operating at wider bandwidths and lower frequencies, for example in the 2-20 MHz region, merely compounds the problem. A general conclusion may therefore be drawn that the distances at which corona from an aircraft might be detected using conventional receiver techniques are not large enough to afford a practical detection system except possibly in the most restricted of environments, and integrating receivers, or radiometers, may afford the only possibility. That is to say, if one postulates

a 5 MHz bandwidth in a receiver operating at 30 MHz, then for the same conditions remaining as in the example above, the distance at which the received power equals the receiver noise power is 1440 Km, or 895 miles. However it is clear that no path and receiving environment are likely to be found over and on which the background noise is not many times the 4 db figure, and therefore such an example is meaningless.

V. CONCLUSIONS AND RECOMMENDATIONS

An early conclusion of this project was to devote major attention and effort to corona discharge rather than to any other possible source of static electrification on aircraft and other airborne devices. It was further concluded that the electromagnetic fields radiated by corona should be the phenomenon of interest, and that appropriate theoretical and experimental studies should be conducted in order to determine the possibility of detection of aircraft by reception and identification of the signals radiated by aircraft undergoing corona.

Precipitation static generated on aircraft by corona discharge has long been recognized as a major problem in the design of noise-free radio communication systems. The local fields produced by the traveling corona current pulses couple strongly to on-board aircraft antennas and produce what is called precipitation static. The radiated field components are negligible by comparison and are not considered an important source of precipitation static noise. Accordingly, little attention has been paid to the radiated fields which accompany the corona discharge process.

Corona discharges occur in the strong local electric field which builds up around the edges of an airframe as the airframe potential rises as a result of the impact of precipitation particles or other charging mechanisms. The discharges create avalanche currents in the air and launch current pulses on the airframe which travel from the discharge point to the open ends of the airframe, where they are reflected. The airframe thus behaves like a pulsed transmission line, and radiates whenever the current pulses encounter a change in impedance due to discontinuities in the geometric or electrical characteristics of the airframe.

During the course of this project, the radiation from a cylinder in corona at one end was measured repeatedly, employing a variety of cylinder

lengths and diameters, and over a broad frequency range with a variety of measuring instruments. These experiments and the results obtained are described in Sections II-C, II-D, and II-G of this report. Because of the low amplitudes of the radiated signals, all measurements were made in the close proximity of the body in corona, in no case at distances greater than fifty feet.

A theoretical analysis was made of the radiated corona pulse, beginning with a solution of Townsend's equation for an electron in a non-uniform electric field between a negatively charged point and a grounded plane and employing a transmission line model of the cylinder on which the corona current is distributed. Good agreement was obtained between the measurements and the theoretical calculations. For example, a power level of -56 dbm was measured at 50 MHz, with the receiving antenna at a distance of 25 feet from a 10 foot pipe in corona. This corresponds to a spectral amplitude of 3.6×10^{-9} volt-seconds/meter at 1 meter. This compares very well with the calculated value of 4.0×10^{-9} volt-seconds/meter for a vertical cylinder over a perfectly conducting ground plane. With the assumption of a random corona discharge rate of 100 kHz, the incident flux density in this case would be 4×10^{-15} watt-seconds/m² at 1 meter, compared to a background noise flux from atmospheric and galactic noise of approximately 1.4×10^{-19} watt-seconds/m² in the 50-100 MHz range. The excellent agreement between measured and calculated values of the radiated corona pulse is a positive result which should encourage further use of the transmission line model in theoretical studies of corona radiation from more complex structures and from actual airframes.

However, the difficulty of making useful corona measurements at significant distances from the source in the presence of man-made background noise is graphically illustrated in Figure 10. Here the background noise

reaches levels as high as -10 dbm, and has an average level of the order of -50 dbm. It is fortuitous that there is a relatively quiet frequency band between approximately 25 and 60 MHz where the noise level is below -70 dbm. It is only in this region where the corona pulse spectrum can be clearly identified, at levels 15 to 20 db above the background. It is therefore clear that in this noise environment, as quiet as could be found in the Denver region, removal of the receiving equipment to 100 feet or greater would result in totally obscuring the corona spectrum in the noise background because of the inverse distance dependence of the radiated electromagnetic field.

It is clear that any possibility of success from a practical point of view in the use of radiated corona signals as a detection mechanism is strongly dependent on the noise background in which such measurements are attempted. This is true whether conventional receiving techniques or special techniques such as the use of integrating noise receivers are employed. A careful and extensive study of background noise is therefore required. An attempt was made on this project to measure natural background noise in what should be quiet regions, far at sea, in the 30 to 350 MHz range. The goal was to record broadband impulsive background noise as well as background noise in narrower bandwidths on a swept frequency basis. The results of this attempt were largely inconclusive since it was not possible to reach distances from shore where television and FM broadcast signals were still not much stronger than the impulsive background noise. Over the frequency range studied, and at the maximum distance reached of 120 miles from shore, man-made noise at levels of -100 dbm predominated. It is suggested that any further research on this method of detection should include varied and carefully controlled experiments in many locations on the exact nature and strength of impulsive background noise in the frequency range of 10-500

MHz. It appears that definitive data are required in this connection, something which proved impossible on this project, before an intelligent assessment can be made of the probabilities of aircraft detection by measurement of corona discharge radiation.

It is also clear that, while a considerable measure of success was achieved in constructing a theoretical model of a cylinder in corona and calculating the radiated electric field pulse, an exact description of the radiated field from an actual aircraft or other airframe in flight in an arbitrary environment would be extremely difficult, if not impossible. Further analytic investigation in this connection is undoubtedly warranted, but care must be exercised that the approximations required do not result in time-consuming calculations which ultimately prove worthless. It would be rather more profitable to make more extensive measurements on actual airframes in corona, in experiments where as many of the parameters as possible can be controlled and understood. This project attempted measurements of this kind, as described in Section II-F. Recordings were made on a 10 MHz narrow-band basis at the relatively quiet frequencies of 150 MHz and 275 MHz approximately 100 meters from the end of a runway at a commercial airport. Signals were received, from a variety of aircraft during rainy periods and from large aircraft during clear periods, and there was good correlation between the passage of an aircraft through the antenna beam and the noise output of the recording system. However, in this case the parameters were not controlled and well understood, and the received noise could not be definitely attributed to corona since no independent means were available to determine whether or not the aircraft were experiencing corona at the time the observations were made. Any future experiments should require exclusive use of a variety of aircraft, operating at a variety of altitudes and in various atmospheric conditions, with on-board instrumentation to

monitor the state and behavior of static electrification, while corona recordings are attempted at a variety of ranges and frequencies. There come to mind such possibilities as tracking aircraft with conventional VHF or UHF radar while they are illuminated with a low-frequency radar receiver operating in the 50-500 MHz range. If the aircraft is known to be in corona, then any received signals would be attributable to that source. It would also be illuminating to place actual aircraft in a laboratory environment and charge them to cause corona at or near the actual corona currents which have been observed while radiation measurements are attempted. Several attempts were made during this project to coordinate with other research and development groups performing static charging tests on aircraft in the Patuxent anechoic hangar; however, such arrangements could never be completed. Had such tests been possible, even though not fully under the control of the DRI experimenters, more conclusive indications of the worth of such experiments would now be available. Such measurements, together with detailed knowledge of the background noise level of the environment, would provide much more definitive evidence than has been heretofore obtained on the possibilities of the use of corona signals.

The use of scale models of actual aircraft and other airframes in experiments such as described above and others is of course immediately attractive. A relatively crude 20:1 scale model of a KC-135 was constructed on this project and corona measurements were made. The chief resonance due to the fuselage as well as several secondary resonances were observed and the average frequency spectrum was seen to fall off sharply above the main resonant frequency. More extensive and more careful experiments using this model were planned but not carried out. Future projects should certainly include the use of models, with a primary goal of an exact specification of the frequency spectrum over as wide a band as is measurable so that the

results could be scaled up to the actual aircraft. These results could then be compared to those obtained on the aircraft itself, and any good agreement obtained would lend credence to further conclusions drawn from model rather than the more expensive actual aircraft tests.

Experiments on this and other projects have conclusively demonstrated the impulsive nature and the repeatability of the corona discharge signal. Since this is the case, it appears possible that special techniques can be developed to pick the corona signal out of the background noise. Such techniques would be especially useful when the background noise did not have impulsive characteristics over the frequency range of interest. That is, assume the time function of the field incident on a receiving antenna to be

$$f(t) = n(t) + m(t),$$

where $n(t)$ is the background noise and $m(t)$ is the signal due to a corona discharge. Suppose $f(t)$ is applied to some system operator at the input of a receiving system such that

$$x(t) = K f(t)$$

where $x(t)$ is the output of this operator. Then if $p(t) = K n(t)$ and $q(t) = K m(t)$ and if K is a linear operator

$$x(t) = p(t) \text{ and } q(t)$$

and it is seen that K should be specified to minimize $p(t)$ and maximize $q(t)$. To realize this goal, both $n(t)$ (the background noise in the vicinity of the receiver) and $m(t)$ (the signal due to corona discharge) must be known. Calculations and measurements show that the lower extreme of the frequency band of $m(t)$ is above the frequencies of AM broadcast signals and atmospheric disturbances due to lightning discharges since it lies at approximately 2 MHz. It is also encouraging that frequencies above approximately 25 MHz are not reflected by the ionosphere so that impulsive background noise above this frequency would be due only to local rather than to distant sources. There-

fore part of the operator K would consist of a high-pass filter with a cut-off frequency at or above 2 MHz, with its remaining composition determined by the nature of the background noise in the vicinity of the receiver and the impulsive shape of the radiated signal from the corona discharge.

Closely allied with the foregoing analysis is the suggestion that it would be advantageous to receive the corona radiation with an integrating type noise receiver known as a radiometer rather than with a conventional receiver. This would make possible the reception of desired impulsive signals at levels below the receiver noise figure and below the background noise level if that background noise is not itself impulsive in nature. Measurements made both of the corona signal itself and of the noise background during this project indicated not only that such an approach might be the only practical one but also provided data from which such a receiver could be specified. Accordingly, such a receiver was designed and built, as described in Section II-G and II-H of this report. However, this approach is valid only when the amplifier noise plus background noise is not impulsive but is reasonably constant over a period corresponding to the required integration time. The receiver was extensively tested and found to meet the design specifications, but all attempts to find a noise environment which was constant and not excessively impulsive in nature failed, and therefore the radiometric principle could not be fairly evaluated on this project. The receiver was therefore used only as a conventional low-noise receiver. The approach, however, remains valid, and it is suggested that future projects should include further examination of the use of radiometers. For example, operating with a controlled corona source such as the aircraft model conventional receivers and radiometers should be compared in performance when used in an environment where the background noise can be controlled or minimized, such as in a shielded room. Then using actual scaled corona signals,

the required frequency range, bandwidth, noise figure, gain, and integration time could be definitely specified.

This project has clearly demonstrated the existence of a radiated electromagnetic field from a body in corona, has calculated its time history and frequency characteristics with reasonable accuracy compared to experimental measurements, and has measured the received pulse in a wide variety of cases in the close proximity of the source. It has also demonstrated that the radiated fields are small at best, and very difficult to detect at large distances. It has shown that serious problems exist in locating receiving environments where the natural noise background is sufficiently low and not impulsive in nature. It indicates that the case is not hopeless, but that extensive further work would be required, particularly experimental data collection on noise background and on actual airframes in corona. Without these, further theoretical investigation would not appear fruitful. It also appears probable that any successful methods would have to employ special receiving techniques such as radiometers rather than conventional receivers. If this is the case, then the questions raised in Appendix A concerning the sensitivity and required integration time of the receiver would have to be resolved by the careful collection and analysis of a considerable body of experimental data on noise background, corona signal strengths, and signal-to-noise ratios.

APPENDIX A

If it is desired to use radiometer type receivers in a study of the signals radiated by corona, then observed data and certain other known parameters can be used to obtain an estimate of the integration times which would be required.

Take the following experimentally obtained data:

20 foot pipe, 2-1/4" diam., in corona

Pipe potential - 8 KV

Single corona point

d-c current < 1-2 μ a

Measured power at receiver - -60 dbm

Antenna distance from source - 16m.

Operating frequency - 50 MHz ($\lambda = 6$ m.)

Bandwidth - 300 kHz

System gain - +5 db at 50 MHz

Then:

Power at antenna load = -65 dbm = -95 dbw

$$= 3.16 \times 10^{-10} \text{ watts}$$

$$= 1.05 \times 10^{-15} \text{ watts/Hz}$$

Antenna gain - $G = 12$ db; $G = 10 \log g$; $g = 15.8$

From antenna theory;

$$W_R = \frac{g\lambda^2}{4\pi} P, \text{ where}$$

W_R = received power measured at antenna load (watts)

$\frac{g\lambda^2}{4\pi}$ = antenna effective area (m^2)

P = incident power density ($watts/m^2$)

Then

$$P = \frac{4\pi W_R}{9\lambda^2} \quad \text{and}$$

$$\text{Incident flux at 16m} = \frac{4\pi \times 1.05 \times 10^{-15}}{15.8(6^2)} = 2.3 \times 10^{-17} \text{ w/m}^2/\text{Hz}$$

$$\text{Incident flux at 1 m.} = (16)^2 \times 2.3 \times 10^{-17} = 5.9 \times 10^{-15} \text{ w/m}^2/\text{Hz}$$

$$\text{at 10 m.} = 5.9 \times 10^{-17}$$

$$\text{at 100 m.} = 5.9 \times 10^{-19}$$

$$\text{at 1 km.} = 5.9 \times 10^{-21}$$

$$\text{at 10 km.} = 5.9 \times 10^{-23}$$

From the literature it is known that:

$$\text{Ambient noise (galactic and atmospheric)} = 10^4 \text{ }^\circ\text{K at 50-100 MHz}$$

$$= 1.4 \times 10^{-19} \text{ w/m}^2/\text{Hz}$$

$$= -120 \text{ dbw in 10 MHz bandwidth}$$

The "Radiometer equation" is

$$\frac{\Delta P}{P_N} \approx \frac{2}{\sqrt{B\tau}}$$

where:

$$P_N \approx \text{ambient noise}$$

$$\Delta P \approx \text{RMS fluctuation of noise}$$

$$B \approx \text{bandwidth in Hz}$$

$$\tau \approx \text{required integration time in seconds.}$$

A signal to be detectable needs to be 3-5 times ΔP .

Take P_s (signal) = 5 ΔP . Then:

$$\frac{P_s}{5P_N} = \frac{2}{\sqrt{B\tau}}$$

$$P_s = \frac{10P_N}{\sqrt{B\tau}} ; B\tau = \frac{100P_N^2}{P_s^2}$$

If there is assumed to be no background noise other than the average galactic and atmospheric noise given above:

$$B\tau = \frac{100(1.4 \times 10^{-19})^2}{P_s^2} = \frac{2 \times 10^{-36}}{P_s^2}$$

We make the following tabulation for required values of τ using the experimental data above: (τ in seconds)

d (meters)	P_s	$B\tau$	τ (B=1MHz)	τ (B=10MHz)	τ (B=20MHz)	τ (B=100MHz)
10	5.9×10^{-17}	5.7×10^{-4}	5.7×10^{-10}	5.7×10^{-11}	2.85×10^{-11}	5.7×10^{-12}
100	5.9×10^{-19}	5.7	5.7×10^{-6}	5.7×10^{-7}	2.85×10^{-7}	5.7×10^{-8}
1 km	5.9×10^{-21}	5.7×10^4	5.7×10^{-2}	5.7×10^{-3}	2.85×10^{-3}	5.7×10^{-2}
5 km	2.4×10^{-22}	3.6×10^7	36	3.6	1.8	0.4
10 km	5.9×10^{-23}	5.7×10^8	5.7×10^2	57	28.5	5.7
100 km	5.9×10^{-25}	5.7×10^{12}	5.7×10^4	5.7×10^3	2.85×10^3	570

Note that for a constant bandwidth τ decreases as the square of signal power. For example, if the aircraft signal power were 10 times the power received from the pipe, then

$$\tau \text{ for } B = 20 \text{ MHz} = 0.285 \text{ sec. at } 10 \text{ km.}$$

The usefulness of these integration times is necessarily subject to extensive experimental investigation because:

1. What real background noise levels will be encountered?
They will certainly be far above the average galactic and atmospheric values used.
2. How will the power received from a 20 foot pipe in corona scale to an actual airframe in flight and experiencing corona?

REFERENCES

1. Schelkunoff, S.A. and Friis, H.T., "Antennas, Theory and Practice," Wiley and Sons, New York, 1952.
2. Raether, H., "Electron Avalanches and Breakdown in Gases," Butterworth and Company, London, 1964.
3. Tamura, T., Proc. Phys. Soc. (Japan), 16, 2503 (1961).
4. Loeb, L.B., "Electrical Coronas, Their Basic Physical Mechanisms," Univ. of Cal. Press, 1965.
5. Jackson, J.D., "Classical Electrodynamics," Wiley and Sons, New York, 1962.
6. Page, L. and Adams, N.I., "Principles of Electricity," D. Van Nostrand Co., New York, 1949.
7. Findley, J.W., "Antennas and Receivers for Radio Astronomy," in "Advances in Radio Research," Vol. 2, (J.A. Saxton, ed.), Academic Press, New York, 1964.
8. Tanner, R.L., and Nanevich, J.E., Proc. IEEE, 52, 44 (1964).

END

FILMED

1-85

DTIC